Biophysical network models of phase-synchronization in MEG resting-state

Williams N[1,2], Toselli B[3], Siebenhühner F[4], Palva S[4,5], Arnulfo G[3], Kaski S[1,6]*, Palva JM[2,4,5]*

Affiliations:
1. Helsinki Institute of Information Technology, Department of Computer Science, Aalto University, Finland
2. Department of Neuroscience & Biomedical Engineering, Aalto University, Finland
3. Department of Informatics, Bioengineering, Robotics & Systems Engineering, University of Genoa, Italy
4. Neuroscience Center, Helsinki Institute of Life Science, University of Helsinki, Finland
5. Centre for Cognitive Neuroimaging, Institute of Neuroscience & Psychology, University of Glasgow, United Kingdom
6. Department of Computer Science, University of Manchester, United Kingdom

* Equally contributing authors

Corresponding author:
Dr. Nitin Williams
Helsinki Institute of Information Technology
Department of Computer Science
Aalto University
Konemiehentie 2
02150, Espoo
Helsinki
Tel: +358 (0)44 919 5512
Email: nitin.williams@aalto.fi

Abstract

Magnetoencephalography (MEG) is used extensively to study functional connectivity (FC) networks of phase-synchronization, but the relationship of these networks to their biophysical substrates is poorly understood. Biophysical Network Models (BNMs) have been used to produce networks corresponding to MEG-derived networks of phase-synchronization, but the roles of inter-regional conduction delays, the structural connectome and dynamics of model of individual brain regions, in obtaining this correspondence remain unknown. In this study, we investigated the roles of conduction delays, the structural connectome, and dynamics of models of individual regions, in obtaining a correspondence between model-generated and MEG-derived networks between left-hemispheric regions. To do this, we compared three BNMs, respectively comprising Wilson-Cowan oscillators interacting with diffusion Magnetic Resonance Imaging (MRI)-based patterns of structural connections through zero delays, constant delays and distance-dependent delays respectively. For the BNM whose networks corresponded most closely to the MEG-derived network, we used comparisons against null models to identify specific features of each model component, *e.g.* the pattern of connections in the structure connectome, that contributed to the observed correspondence. The Wilson-Cowan zero delays model produced networks with a closer correspondence to the MEG-derived network than those produced by the constant delays model, and the same as those produced by the distance-dependent delays model. Hence, there is no evidence that including conduction delays improves the correspondence between model-generated and MEG-derived networks. Given this, we chose the Wilson-Cowan zero delays model for further investigation. Comparing the Wilson-Cowan zero delays model against null models revealed that both the pattern of structural connections and Wilson-Cowan oscillatory dynamics contribute to the correspondence between model-generated and MEG-derived networks. Our investigations yield insight into the roles of conduction delays, the structural connectome and dynamics of models of individual brain regions, in obtaining a correspondence between model-generated and MEG-derived networks. These findings result in a parsimonious BNM that produces networks corresponding closely to MEG-derived networks of phase-synchronization.

Keywords: Biophysical Network Models; Wilson-Cowan oscillators; Phase-synchronization; Magnetoencephalography; MEG resting-state; MEG functional networks

73 **Highlights**

74 • Simple biophysical model produces close match ($\rho=0.49$) between model and MEG

75 networks

76 • No evidence for conduction delays improving match between model and MEG

77 networks

78 • Pattern of structural connections contributes to match between model and MEG

79 networks

80 • Wilson-Cowan oscillatory dynamics contribute to match between model and MEG

81 networks

82

83

84

85

86

87

88

89

90

91

92

93

94

95

96

97

98

99

100

101

102

1. Introduction

103

104 Functional Connectivity (FC) networks underpin the execution of cognitive tasks (Cole et al.
105 (2013), Cohen & D'Esposito (2016)) and are also observed during resting-state (Beckmann et
106 al. (2005), Damoiseaux et al. (2006)). FC networks are sets of interacting brain regions,
107 wherein the interactions are reflected by correlated activities of the brain regions. Key forms
108 of correlation observed in Electroencephalography (EEG) and Magnetoencephalography
109 (MEG) resting-state or task data, are the pairwise correlations between the oscillation
110 amplitudes of a set of brain regions (Hipp et al. (2012), Colclough et al. (2015), Brookes et al.
111 (2012)), or the pairwise synchronization between oscillation phases of a set of brain regions
112 (Palva et al. (2005), Palva et al. (2010), Palva & Palva (2012), Zhigalov et al. (2015),
113 Siebenhühner et al. (2020), Marzetti et al. (2019)). FC networks of amplitude correlation or
114 phase-synchronization are widely studied with EEG/MEG, but the structure-function mapping
115 between biophysical substrates and FC networks is poorly understood. We refer to biophysical
116 substrates as systems-level components, *e.g*., the structural connectome, dynamics of brain
117 regions or inter-regional conduction delays, which underpin observed FC networks.

118

119 Biophysical Network Models (BNMs) (Woolrich & Stephan (2013)) have been used to relate
120 MEG-derived networks of amplitude correlation to their biophysical substrates. BNMs
121 comprise models of individual brain regions, linked by biologically informed structural
122 connectivity. BNMs of Kuramoto oscillators linked by diffusion Magnetic Resonance Imaging
123 (dMRI)-based structural connections with realistic conduction delays, produced FC networks
124 of amplitude correlation corresponding moderately to those observed in MEG resting-state
125 (Cabral et al. (2014)) ($\rho = 0.41$, where ρ is Pearson Correlation). Similarly, BNMs of spiking
126 neuron populations linked by dMRI-based structural connections with realistic delays also
127 produced FC networks of amplitude correlation corresponding moderately to those observed
128 in MEG-derived networks of amplitude correlation ($\rho = 0.4$) (Nakagawa et al. (2014)).

129

130 FC networks of phase-synchronization have been suggested to be relevant to information
131 processing in the brain, coordinating communication across regions via regulation of spike-
132 time relationships (Fries (2005), Singer (1999), Palva & Palva (2012)) and supporting
133 functional integration (Palva & Palva, (2012), Siegel et al. (2012), Deco et al. (2015)). In fact,
134 particular phase-synchronization networks are known to be recruited for specific cognitive

135   tasks, including working memory (Kitzbichler et al. (2011), Palva et al. (2010)), visual

136   attention (Lobier et al. (2018)) and sensorimotor processing tasks (Hirvonen et al. (2018)).

137

138   Just as for MEG-derived networks of amplitude correlation, BNMs have been employed to

139   relate EEG- or MEG-derived networks of phase-synchronization to their biophysical

140   substrates. BNMs of Kuramoto oscillators linked by dMRI-based structural connections with

141   conduction delays, produced networks of phase-synchronization corresponding to those

142   observed in EEG resting-state (Finger et al. (2016)). However, this model produced networks

143   with only weak correspondence to EEG-derived networks, when the networks were estimated

144   with measures insensitive to EEG volume conduction ($\rho = 0.17$ for weighted Phase Lag Index

145   (wPLI)). BNMs of Wilson-Cowan oscillators with inhibitory synaptic plasticity (ISP), linked

146   by dMRI-based structural connections with conduction delays, have been used to produce

147   networks of phase-synchronization corresponding to those observed in MEG resting-state

148   (Abeysuriya et al. (2018)). While this BNM produced networks with a moderate correlation to

149   MEG-derived networks ($\rho = 0.43$ for Phase Locking Value (PLV), $\rho = 0.28$ for Phase Lag

150   Index (PLI)) (Abeysuriya et al. (2018)), the strengths of model-generated phase-

151   synchronization (~0 - 0.6 for PLV and ~0 - 1 for PLI) were an order of magnitude higher than

152   those observed in MEG-derived networks (~0.01 - 0.06 for both PLV and PLI). Further, while

153   the correspondence between the model-generated and MEG-derived networks was assessed,

154   the roles of conduction delays, the structural connectome and the dynamics of models of

155   individual brain regions in producing this correspondence was not investigated.

156

157   In this study, we investigated the roles of conduction delays, the structural connectome and the

158   dynamics of models of individual regions, in producing networks corresponding to observed

159   MEG-derived networks of phase-synchronization between left-hemispheric regions. To do

160   this, we first compared three hypotheses, respectively postulating model-generated networks

161   of phase-synchronization corresponding to MEG-derived networks, are produced by the

162   dynamics of Wilson-Cowan oscillators linked by dMRI-based patterns of structural

163   connections, via zero, constant and distance-dependent conduction delays. We expressed each

164   of these hypotheses as a BNM. For the BNM producing networks corresponding most closely

165   to the observed MEG-derived networks, we used comparisons against null models to determine

166   specific features of each model component, for *e.g.,* pattern of connections in the structural

167   connectome, that contribute to the correspondence between the model-generated and MEG-

168   derived networks. Together, these investigations yield insight into the precise roles of inter-

169   regional conduction delays, the structural connectome and the dynamics of models of

170   individual brain regions, in producing networks corresponding to observed MEG-derived

171   networks of phase-synchronization.

172   2. Materials & Methods

173   In this study, we investigated the roles of conduction delays, the structural connectome and the

174   dynamics of models of individual brain regions, in producing model-generated networks

175   corresponding to the observed MEG-derived networks of phase-synchronization. To do this,

176   we first compared the correspondence between model-generated and MEG-derived networks

177   of three BNMs, respectively including zero, constant and distance-dependent conduction

178   delays. Figure 1 illustrates the pipeline to estimate and compare the model-generated and MEG-

179   derived networks. For the BNM producing networks corresponding most closely to the MEG-

180   derived networks, we used null models to determine specific features of each model component

181   that contributes to the correspondence between model-generated and MEG-derived networks.

182   For example, we compared the correspondence between model-generated networks from the

183   original model and the MEG-derived networks, against the correspondence between model-

184   generated networks from null models comprising degree-preserved randomised versions of the

185   structural connectome, and the MEG-derived networks. Such a comparison enabled inferences

186   on the contribution of the *pattern* of structural connections to the correspondence between

187   model-generated and MEG-derived networks, over and above the number of connections, *i.e.*

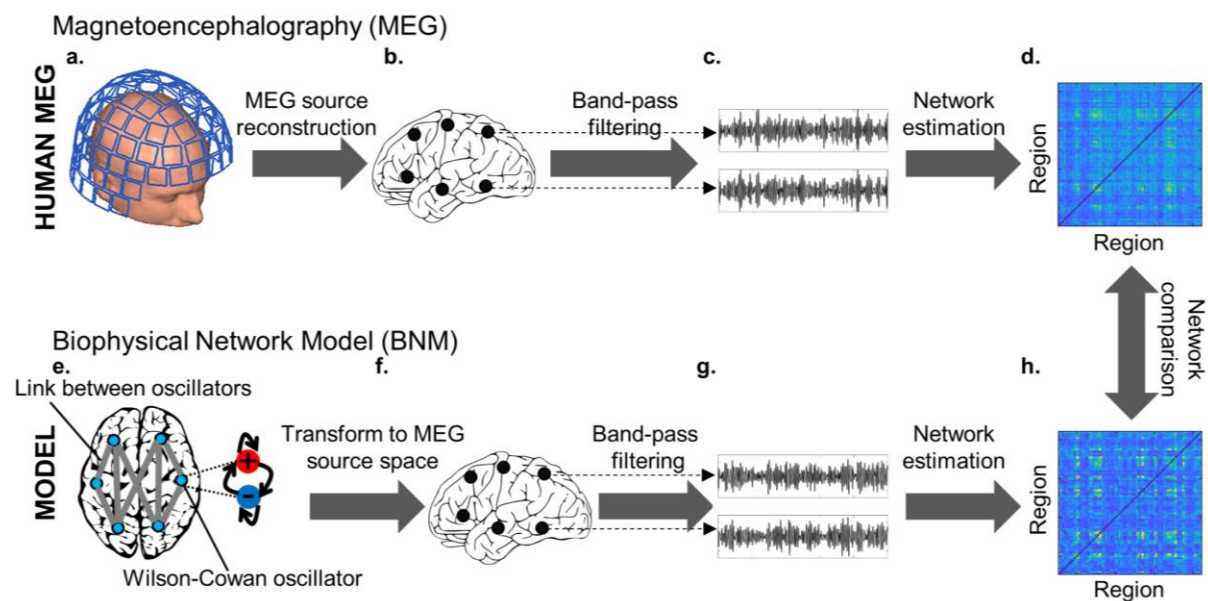188   degree, to each brain region.

189

Figure 1. Pipeline to generate and compare model-generated and MEG-derived networks of phase-synchronization. a. MEG device with sensors detecting weak magnetic fields arising from post-synaptic potentials in the human brain. b. Source-reconstructed data projected from MEG sensors to brain regions. c. Band-pass filtered source-reconstructed MEG data. d. Matrix of strength of phase-synchronization between source-reconstructed MEG data from every pair of brain regions. e. Biophysical Network Model (BNM) comprising Wilson-Cowan oscillators linked by biologically informed structural connections. f. Simulated data transformed to MEG source space by projecting dynamics to MEG sensors, and projecting sensor-level simulated data back to brain regions. g. Band-pass filtered source-reconstructed simulated MEG data. h. Matrix of strength of phase-synchronization between source-reconstructed simulated MEG data from every pair of brain regions. MEG device panel from Pfeiffer et al. (2018).

2.1. Models

We implemented three models, each representing specific hypotheses on the interaction between dynamics of models of brain regions, structural connectome and conduction delays, in producing networks corresponding to MEG-derived networks of phase-synchronization.

Wilson-Cowan zero delays model: Wilson-Cowan oscillatory dynamics interact with the pattern of connections in the structural connectome without conduction delays, to produce networks of phase-synchronization corresponding to those observed in MEG resting-state.

212 We implemented this model as a set of Wilson-Cowan oscillators linked by biologically

213 informed structural connectivity (Wilson & Cowan (1972), Kilpatrick (2013), Cowan (2016)).

214 The dynamics of each oscillator arise from the interaction between excitatory and inhibitory

215 neuronal populations, *i.e.* the PING model (Traub et al. (1997)), and are also influenced by

216 external inputs and the dynamics of linked oscillators. For oscillator i:

217
$$\tau_e \frac{dU_e}{dt} = -U_e(t) + F(w_{ee}U_e(t) - w_{ei}U_i(t) - b_e + J_e + k\sum_{j=1}^{N} K(i,j)U_e(t))$$

218
$$\tau_i \frac{dU_i}{dt} = -U_i(t) + F(w_{ie}U_e(t) - w_{ii}U_i(t) - b_i + J_i)$$

219

220 where $F(v) = \frac{1}{1+e^{-v}}$ is a sigmoid function, $U_e(t)$ and $U_i(t)$ are the mean firing rates at time

221 t of the excitatory and inhibitory populations respectively, w_{ee} and w_{ii} are the excitatory-

222 excitatory and inhibitory-inhibitory connection weights respectively, w_{ie} and w_{ei} are the

223 excitatory-inhibitory and inhibitory-excitatory connection weights, b_e and b_i are threshold

224 constants for excitatory and inhibitory populations, J_e and J_i are injection currents to excitatory

225 and inhibitory populations, τ_e and τ_i are the time constants of the excitatory and inhibitory

226 populations, and k is a scalar multiplier over the coupling matrix K, which specifies links

227 between N oscillators. For this model, we postulated that non-zero conduction delays are not

228 relevant to producing the networks of phase-synchronization observed in MEG resting-state.

229

230 *Parameter values*: We set the parameters of each Wilson-Cowan oscillator to the same values

231 (Table 1) since we assumed the intrinsic properties of the brain regions are identical. The choice

232 of values for connection weights within (w_{ee}, w_{ii}) and between (w_{ie}, w_{ei}) excitatory and

233 inhibitory populations, and the strengths of external currents (J_e, J_i) are consistent with

234 canonical neurophysiological findings of 1.) strong excitatory-excitatory connections (Jansen

235 & Rit (1995), Douglas et al. (1989), Binzegger et al. (2004)) 2.) excitatory-inhibitory and

236 inhibitory-excitatory connections being weaker than excitatory-excitatory connections (Jansen

237 & Rit (1995), Binzegger et al. (2004)) 3.) weak inhibitory-inhibitory connections (Douglas et

238 al. (1989), Binzegger et al. (2004)) and 4.) the strength of injection currents, *e.g.* from thalamus,

239 being significantly lower than strength of excitatory-excitatory connections (Douglas et al.

240 (1989), Binzegger et al. (2004)). The threshold constants of excitatory (b_e) and inhibitory

241 populations (b_i) are difficult to determine from the neurophysiology literature, but the values

242 were chosen to produce oscillatory phenomena (Wilson & Cowan (1972), Singh et al. (2016),

243   Sreenivasan et al. (2017)). We chose the excitatory (τ_e) and inhibitory time constants (τ_i) to

244   produce dynamics around 10 Hz, *i.e.* the peak frequency of oscillatory power in the power

245   spectrum of MEG resting-state (Nakagawa et al. (2014)). We tuned the parameter k, *i.e.* the

246   scalar multiplier over the coupling matrix, K (see Section 2.6).

247

Parameters	Values
$w_{ee}, w_{ii}, w_{ie}, w_{ei}$	16, 3, 12, 15
b_e, b_i	4, 3.7
J_e, J_i	2, 0
τ_e, τ_i	23.7, 23.7

248

249   **Table 1.** Parameter values of individual Wilson-Cowan oscillators

250

251   *Wilson-Cowan constant delays model*: Wilson-Cowan oscillatory dynamics interact with the

252   pattern of connections in the structural connectome through constant non-zero conduction

253   delays, to produce networks of phase-synchronization corresponding to those observed in MEG

254   resting-state.

255

256   We implemented this model as a set of Wilson-Cowan oscillators linked by biologically

257   informed structural connectivity with constant, non-zero delays. The dynamics of individual

258   oscillators were influenced by inter-regional interactions of constant delay, in contrast to zero

259   delays assumed by the Wilson-Cowan zero delays model. For oscillator i:

260
$$\tau_e \frac{dU_e}{dt} = -U_e(t) + F(w_{ee}U_e(t) - w_{ei}U_i(t) - b_e + J_e + k \sum_{j=1}^{N} K(i,j)U_e(t-T))$$

261
$$\tau_i \frac{dU_i}{dt} = -U_i(t) + F(w_{ie}U_e(t) - w_{ii}U_i(t) - b_i + J_i)$$

262

263   where T specifies the constant delay in milliseconds, and all other terms bear the same

264   definitions as the Wilson-Cowan zero delays model. For this model, we postulated that the

265   increase in conduction delay due to longer distance between regions is counteracted by the

266   decrease in conduction delay due to higher conduction velocity between regions. This

267   assumption is supported by recent modelling work (Noori et al. (2020)) reporting highly similar

268   conduction delays across region-pairs due to increased conduction velocity produced by

269   activity-dependent myelination counteracting longer delays between distant brain regions.

270

271   *Parameters values*: We set the parameters of the Wilson-Cowan oscillators to the values in

272   Table 1, and tuned the parameters k and constant delay T (see Section 2.6).

273

274   *Wilson-Cowan distance-dependent delays model*: Wilson-Cowan oscillatory dynamics interact

275   with the pattern of connections in the structural connectome through distance-dependent

276   conduction delays, to produce networks of phase-synchronization corresponding to those

277   observed in MEG resting-state.

278

279   We implemented the Wilson-Cowan distance-dependent delays model as comprising a set of

280   Wilson-Cowan oscillators linked by biologically informed structural connectivity, with

281   conduction delays proportional to distance between respective brain regions. The dynamics of

282   individual oscillators are influenced by inter-regional interactions of variable delay, in contrast

283   to zero and constant delays assumed by the Wilson-Cowan zero delays and constant delays

284   models respectively. For oscillator i:

285    $$\tau_e \frac{dU_e}{dt} = -U_e(t) + F(w_{ee}U_e(t) - w_{ei}U_i(t) - b_e + J_e + k \sum_{j=1}^{N} K(i,j)U_e(t - T(i,j)))$$

286    $$\tau_i \frac{dU_i}{dt} = -U_i(t) + F(w_{ie}U_e(t) - w_{ii}U_i(t) - b_i + J_i)$$

287

288   where $T(i,j)$ specifies the distance-dependent delay in metres/second, and all other terms bear

289   the same definitions as the model describing the Wilson-Cowan zero delays model. For this

290   model, we specified conduction delays as Euclidean distance between regions divided by a

291   conduction velocity v (Cabral et al. (2014), Nakagawa et al. (2014), Hadida et al. (2018)).

292

293   Rather than Euclidean distance, an alternative method to estimate distances between brain

294   regions is the average length of the streamlines between regions, as calculated by the

295   tractography method used. However, we found the average estimated streamline lengths of

296   ~20% of structural connections to be lower than the corresponding Euclidean distances, which

297   represent the minimum length between regions. Since this might be due to known biases in

298 streamline termination with tractography methods (Smith et al. (2013)), we chose Euclidean

299 distance to estimate distances between brain regions.

300

301 *Parameters values*: We set the parameters of the Wilson-Cowan oscillators to the values in

302 Table 1, and tuned the parameters k and the conduction velocity v (see Section 2.6).

303

304 **2.2. Model comparison**

305 We compared the Wilson-Cowan zero delays, constant delays and distance-dependent delays

306 models by the correspondence between their respective networks of phase-synchronization and

307 the observed MEG-derived network of phase-synchronization. We ran 20 simulations of each

308 model to obtain its dynamics at different starting conditions. After each run, we compared the

309 model-generated network of phase-synchronization to a held-out MEG-derived network of

310 phase-synchronization, *i.e.* an MEG-derived network not used to estimate model parameters

311 (see Section 2.5). We quantified correspondence between model-generated and MEG-derived

312 networks, *i.e.* model performance, by the RMSE (Root Mean Square Error) and Pearson

313 Correlation between the upper-triangular elements of the model-generated and MEG-derived

314 adjacency matrices, low RMSE and high Correlation reflecting a close correspondence. We

315 used independent samples *t*-tests of the respective RMSE and Correlation values to compare

316 model performances, with two-tailed $p < 0.001$ considered statistically significant. Further, we

317 used Cohen's *d* (Cohen (1988)) to measure effect sizes, with $d \geq 1$ considered a strong effect.

318

319 **2.3 Obtaining model-generated network of phase-synchronization**

320 Below, we describe the details of the different model components, model simulations, and the

321 procedure to generate the network of phase-synchronization from the model dynamics.

322

323 **2.3.1 Model elements**

324 The model comprised an ensemble of 74 Wilson-Cowan oscillators linked by biologically

325 informed structural connectivity. We used the left-hemispheric regions of the Destrieux brain

326 atlas (Destrieux et al. (2010)) to specify the number and location of the oscillators. We specified

327 the links between oscillators by the binary matrix of the strongest 10 percentile structural

328 connections between left-hemispheric regions of the Destrieux atlas. We derived this binary

329 matrix from a group-averaged (N=57) weighted matrix of the number of streamlines between

330 brain regions, estimated by constrained spherical deconvolution (Smith et al. (2013)) and

331 probabilistic tractography (Smith et al. (2012)) on pre-processed DWI images from the Human

332   Connectome Project (van Essen et al. (2013)). We divided each element of the binary matrix

333   by the sum of elements in its row, to ensure similar strengths of inputs to each of the 74 regions

334   (Hlinka & Coombes (2012), Forrester et al. (2020)).

335

336   **2.3.2 Model simulations**

337   We used the Brain Dynamics Toolbox (BDT) for model simulations (Heitmann et al. (2018)).

338   The Wilson-Cowan zero delays model is implemented in BDT, while we extended the BDT

339   implementation of the zero delays model to implement the Wilson-Cowan constant delays and

340   Wilson-Cowan distance-dependent delays models. We have made these implementations

341   publicly available (Williams et al. (2021a)). We simulated the models for 630 seconds at 500

342   Hz with ODE45 (Bogacki & Shampine (1996)) for the Wilson-Cowan zero delays model, and

343   ODE23a (Shampine & Thompson (2001)) for the constant delays and distance-dependent

344   delays models. We limited local discretisation error by setting Absolute and Relative Tolerance

345   of all solvers to 1×10^{-6} and 1×10^{-3} respectively. We set initial conditions of excitatory and

346   inhibitory populations of the Wilson-Cowan oscillators by sampling a uniform random

347   distribution between 0 and 1. Notably, we used dynamics of only the excitatory populations for

348   further processing since pyramidal neurons in excitatory populations are the dominant

349   contributors to the measured MEG (Lopes da Silva (2013)). These model dynamics represented

350   the mean firing rate of pyramidal neurons in excitatory populations.

351

352   **2.3.3 Transforming simulated data to MEG source-space**

353   We transformed simulated data to MEG source-space by forward-projecting the simulated data

354   to MEG sensors and then inverse-projecting the simulated sensor-level data, with subject-

355   specific forward and inverse operators respectively (Korhonen et al. (2014)). We used the same

356   forward and inverse operators estimated to source-reconstruct the sensor-level MEG resting-

357   state data (see Section 2.4.2). This procedure yielded subject-specific source-reconstructed

358   simulated MEG datasets, of activity from 74 regions for 630 seconds.

359

360   **2.3.4 Band-pass filtering**

361   We band-pass filtered the model dynamics in the alpha frequency band (8 - 12 Hz) since it is

362   the dominant source of oscillatory power in MEG resting-state (Nakagawa et al. (2014)). We

363   performed the filtering with Morlet wavelets of peak frequency = 9.83 Hz, width parameter =

364   5, yielding subject-specific narrowband datasets, from 74 regions for 630 seconds.

365

2.3.5 Estimating network of phase-synchronization

For each subject-specific dataset, we used weighted Phase Lag Index (wPLI) (Vinck et al. (2011)) to estimate strength of phase-synchronization between each pair of brain regions.

$$wPLI = \frac{|E(|Imag(X)|sign(Imag(X)))|}{E(|Imag(X)|)}$$

where X is the cross-spectrum between a pair of signals and $Imag(X)$ is its imaginary component. Crucially, wPLI is insensitive to the confounding influence of MEG field spread (Vinck et al. (2011), Palva et al. (2018)). We removed the effect of transient dynamics on the phase-synchronization estimates by discarding the first 30 seconds of each dataset. The phase-synchronization estimation produced 74×74 subject-specific matrices, which we averaged to obtain the model-generated network of phase-synchronization.

2.4 Obtaining MEG-derived network of phase-synchronization

Below, we describe the details of acquiring, preprocessing, source-reconstructing sensor-level MEG resting-state data and estimating the MEG-derived network of phase-synchronization.

2.4.1 Data acquisition & pre-processing

We recorded MEG resting-state data from 46 healthy subjects (19 female, age 30.7 ± 9.5 years) for 600 seconds at a sampling rate of 1000 Hz. During the recordings, we instructed subjects to focus on a cross on the screen in front of them during the recordings. We performed the recordings at Meilahti hospital, Helsinki with a 306-channel MEG system (204 planar gradiometers and 102 magnetometers, MEGIN Oy). For each subject, we collected T1-weighted anatomical MRI scans at a resolution of $1 \times 1 \times 1$ mm with a 1.5T MRI scanner (Siemens, Germany). The Ethics Committee of Helsinki University Central Hospital approved the study, and we performed the study according to the Declaration of Helsinki. We obtained written informed consent from each participant. We used MaxFilter (Taulu & Hari (2009)) to suppress extra-cranial noise and co-localise the sensor-space recordings, and Independent Component Analysis (ICA) (Oostenveld et al. (2011)), to exclude components identified as ocular or cardiac artefacts.

2.4.2 Estimating MEG-derived network of phase-synchronization

We transformed preprocessed, sensor-level MEG data time series to brain regions, then band-pass filtered these data and estimated networks of phase-synchronization. We used MNE software to generate subject-specific inverse operators (Hämäläinen & Ilmoniemi (1994)) to transform sensor-level data to the level of cortical parcels or brain regions (Palva et al. (2010), Zhigalov et al. (2017), Lobier et al. (2018), Hirvonen et al. (2018)). We applied fidelity weighting (Korhonen et al. (2014)) on the inverse operators to reduce the influence of MEG field spread. We also used MNE to generate subject-specific forward operators, including subject-specific head conductivity models, cortically constrained source models with 5000-7500 sources per hemisphere, and to co-localise MEG to MRI. We used FreeSurfer (http://surfer.nmr.mgh.harvard.edu/) for volumetric segmentation of MRI data, surface reconstruction, flattening, cortical parcellation and neuroanatomical labelling of each source to a region in the Destrieux brain atlas. For each subject, we averaged the time series of sources within a region to obtain the activity time-course for that region. We then downsampled each subject-specific dataset to 500 Hz and retained the time courses of the 74 left-hemispheric regions for further processing. We used an identical procedure as applied to the simulated data, to perform band-pass filtering (see Section 2.3.4) and to estimate subject-specific 74×74 MEG-derived matrices of phase-synchronization (see Section 2.3.5).

2.5 Splitting MEG-derived networks into training and testing datasets

We generated two subsets of the original 46 subject-specific phase-synchronization matrices, to estimate free model parameters and to evaluate model performance respectively. The first subset or training dataset contained 23 unique, randomly selected subject-specific matrices. We averaged the matrices to obtain a group-level matrix, which we used as the target MEG-derived network to estimate model parameters. The held-out or testing dataset contained the 23 subject-specific matrices not used in the first subset. We averaged these matrices to obtain a group-level matrix, which we used as the target MEG-derived network to determine correspondence between model-generated and MEG-derived networks.

2.6 Determining optimal values of model parameters

We selected optimal model parameter values by performing a grid search for a range of parameter values. We quantified correspondence between model-generated and MEG-derived networks, *i.e.,* model performance, as RMSE and Pearson Correlation between the upper-triangular elements of the model-generated and the training set MEG-derived matrices of

433   phase-synchronization (see Section 2.5). We chose optimal parameter values as those

434   simultaneously yielding low RMSE and high Correlation. For the zero delays, constant delays

435   and distance-dependent delays models, we used the parameter range of $k = 0.5$ to 5, in intervals

436   of 0.5, for the scalar multiplier over the structural connectome. For the constant delays model,

437   we had a delay parameter T, with range from 2 ms to 20 ms, in intervals of 2 ms. For the

438   distance-dependent delays model, we had a conduction velocity parameter v, with range from

439   3 m/s to 30 m/s, in intervals of 3 m/s. We ran simulations for 315 seconds for each parameter

440   combination and discarded the first 30 seconds to remove transient model dynamics, before

441   estimating the model-generated network of phase-synchronization.

442

443   **2.7 Evaluating statistical significance of model performance**

444   We evaluated statistical significance of model performance by comparing against permutation-

445   based null distributions of the performance measures. We quantified model performance by

446   RMSE and Correlation between upper-triangular elements of the mean model-generated matrix

447   of phase-synchronization and the held-out testing set MEG-derived matrix of phase-

448   synchronization (see Section 2.5). We estimated the mean model-generated matrix of phase-

449   synchronization by averaging the 20 model-generated matrices from different starting

450   conditions. We determined statistical significance of the RMSE and Correlation values by z-

451   scoring them against 100 corresponding values estimated after randomly permuting, without

452   replacement, the mean model-generated matrix. We tested the hypotheses that RMSE is lower

453   than chance and that Correlation is higher than chance by calculating the one-tailed p-value of

454   the z-scores, with $p < 0.001$ considered statistically significant.

455

456   **2.8 Sensitivity of model performance to choice of model parameter values**

457   We assessed the sensitivity of the model's performance to small changes in parameter values.

458   To do this, we determined RMSE and Correlation values between the MEG-derived matrix and

459   model-generated matrices generated from simulating jittered models. To introduce jitter, each

460   non-zero parameter of the model was varied between -10% and 10% of its original value, with

461   2% increments, while keeping all other parameters at their original values. Then, we z-scored

462   the RMSE and Correlation values against the 20 RMSE and Correlation values from the

463   original model. z values higher than 3 were considered to reflect values of parameters at which

464   the model performance was sensitive.

465

466

2.9 Determining features of each model component contributing to model performance

467

468 For the model producing networks of phase-synchronization corresponding most closely to the

469 MEG-derived networks of phase-synchronization, we determined specific features of each

470 model component, *e.g.,* pattern of connections in the structural connectome, contributing to the

471 observed correspondence. To do this, we compared the correspondence between model-

472 generated and MEG-derived networks obtained with the original model, against the

473 correspondence obtained with 100 examples of a null model, each containing a randomised

474 version of a specific model component, *e.g.,* randomly connected structural connectome, while

475 all other aspects of the model remained identical to the original model.

476

477 Each of the Wilson-Cowan zero delays, constant delays and distance-dependent delays models,

478 postulate that the topological organisation of the structural connectome, *i.e.,* its pattern of

479 connections, contributes to the correspondence between model-generated and MEG-derived

480 networks. To verify this, we created 100 examples of a null model containing degree-preserved

481 but randomised versions (Maslow & Sneppen (2002)) of the original binary structural

482 connectome, while all other aspects were identical to the original model. For each example of

483 this null model, the randomised structural connectome had the same number of connections to

484 each brain region as the original structural connectome, but the pattern of connections between

485 regions was different to the original structural connectome. By comparing the correspondence

486 between model-generated and MEG-derived networks of the original model against the

487 correspondences obtained with the null models, we tested the hypothesis that the pattern of

488 structural connections contributed to the observed correspondence, over and above the number

489 of connections, *i.e.,* degree, to each brain region.

490

491 Each of the Wilson-Cowan zero delays, constant delays and distance-dependent delays models

492 postulate that the Wilson-Cowan oscillatory dynamics contribute to the correspondence

493 between model-generated and MEG-derived networks. To verify this, we created 100 examples

494 of a null model where the dynamics of each brain region were described by a uniform random

495 distribution whose mean (0.2) and range (0.07 to 0.36) were matched to those of original

496 Wilson-Cowan dynamics, while the original structural connectome specified the interaction

497 between regions. The model is specified as:

498
$$\frac{dU}{dt} = -U(t) + F(rand(t) + k \sum_{j=1}^{N} K(i,j)U(t - T(i,j)))$$

499 where $F(v) = \frac{1}{1+e^{-v}}$ is a sigmoid function, $U(t)$ is the mean firing rate, $rand(t)$ is a sample

500 from a uniform random distribution, k is a scalar multiplier over the coupling matrix K, which

501 specifies links between N oscillators and $T(i,j)$ is a delay matrix containing zeros for all

502 elements, for the Wilson-Cowan zero delays model, a constant non-zero delay for all elements,

503 for the Wilson-Cowan constant delays model, and connection-specific delays for each element,

504 for the Wilson-Cowan distance-dependent delays model. We estimated the parameter k using

505 the same procedure as for the original model (see Section 2.6). We set Relative Tolerance of

506 the simulation to 0.1, to ensure completion in a reasonable time. By comparing the

507 correspondence between model-generated and MEG-derived networks of the original model

508 against the correspondences obtained with the null models, we tested the hypothesis that the

509 Wilson-Cowan oscillatory dynamics contributed to the correspondence between model-

510 generated and MEG-derived networks of phase-synchronization, over and above random

511 dynamics with same mean and range as the Wilson-Cowan oscillatory dynamics.

512

513 The Wilson-Cowan distance-dependent delays model postulated that the connection-specific

514 delays contributed to the correspondence between the model-generated and MEG-derived

515 networks. To verify this, we created 100 examples of a null model by randomly permuting

516 delays (without replacement) from the original model, while all other aspects, including the

517 structural connectome and Wilson-Cowan oscillatory dynamics, were identical to the original

518 model. By comparing the correspondence between model-generated and MEG-derived

519 networks of the original model against the correspondences obtained with the null models, we

520 tested the hypothesis that the connection-specific delays contributed to the observed

521 correspondence, over and above merely the set of conduction delays used. Since the Wilson-

522 Cowan zero delays and Wilson-Cowan constant delays models had the same delays for each

523 connection, determining the contribution of connection-specific delays to the correspondence

524 between model-generated and MEG-derived networks was not relevant.

525

526 Correspondence between the model-generated and MEG-derived networks, for both the

527 original model and null models, were quantified by RMSE and Correlation between the upper-

528 triangular elements of model-generated and the testing set MEG-derived matrices of phase-

529 synchronization (see Section 2.5). To remove outliers from the null distribution, we excluded

530 cases for which RMSE values lay more than 5SD from the mean. We then estimated the *z*-
531 score of the original model's RMSE and Correlation against RMSE and Correlation of the null
532 models. We tested the hypotheses that mean RMSE for the original model is lower than RMSE
533 for the null models and mean Correlation for the original model is higher than Correlation for
534 the null models by calculating one-tailed p-values of the respective *z*-scores, with $p < 0.001$
535 considered a statistically significant contribution.

536

537 **2.10 Comparing model performance against performance of Kuramoto oscillator model**
538 For the model producing networks of phase-synchronization corresponding most closely to
539 those observed in MEG resting-state, we compared its observed correspondence against the
540 correspondence between model-generated and MEG-derived networks of an equivalent
541 Kuramoto oscillator model (Kuramoto (1984)). The Kuramoto oscillator model has been used
542 to model oscillatory phenomena in systems neuroscience (Breakspear et al. (2010), Cabral et
543 al. (2014)). The phase dynamics of individual regions were described by the classic Kuramoto
544 model, where we used the same coupling matrix K as in the Wilson-Cowan models, to specify
545 links between regions. The sine of instantaneous phases was computed to convert the phase
546 dynamics to time series of oscillatory activity. We set the scalar multiplier k over the coupling
547 matrix with the same training procedure used for the Wilson-Cowan zero delays model (Section
548 2.6), while we set the natural frequencies of the Kuramoto oscillators so as to produce
549 oscillatory dynamics around 10 Hz. To do this, we set the natural frequencies as independent
550 samples from a Gaussian distribution of mean $= 6.2 \times 10^{-2}$ and standard deviation $= 6.2 \times$
551 10^{-3}. We simulated the model, then applied the same processing as to the Wilson-Cowan
552 model dynamics (see Section 2.3) to furnish the Kuramoto model-generated matrix of phase-
553 synchronization, which we then matched to the MEG-derived matrix with RMSE and
554 Correlation. We used independent samples *t*-tests to compare RMSE and Correlation values of
555 the chosen model against RMSE and Correlation values of the Kuramoto model, with two-
556 tailed $p < 0.001$ considered statistically significant.

557 3. Results

558 3.1 Determining optimal values of model parameters
559 We estimated the optimal values of free parameters, for the Wilson-Cowan zero delays,
560 constant delays and distance-dependent delays models. We identified the optimal parameter

561   values as those that yielded model-generated matrices of phase-synchronization with the
562   strongest correspondence to the training set MEG-derived matrices of phase-synchronization.
563   For each of the models, we compared model-generated and MEG-derived matrices of phase-
564   synchronization using RMSE and Pearson Correlation, choosing parameter values yielding low
565   RMSE and high Correlation (Figure 2). For the Wilson-Cowan zero delays model, the optimal
566   parameter value is $k = 2$, yielding RMSE = 0.04 and Correlation = 0.45, k being the scalar
567   multiplier over the structural connectome. For the Wilson-Cowan constant delays model, the
568   optimal combination of parameter values is $k = 2$ and $T = 2$ ms, yielding RMSE = 0.04 and
569   Correlation = 0.33, with T being the constant delay between brain regions. For the Wilson-
570   Cowan distance-dependent delays model, the optimal combination of parameter values is $k =$
571   1.5 and $v = 12$ m/s, yielding RMSE = 0.04 and Correlation = 0.38, with v being the assumed
572   transmission velocity of neuronal activity across structural connections. We used these values
573   to run fresh simulations of the Wilson-Cowan zero delays, constant delays and distance-
574   dependent delays models, and determined correspondences of the respective model-generated
575   matrices of phase-synchronization to the testing set MEG-derived matrix of phase-
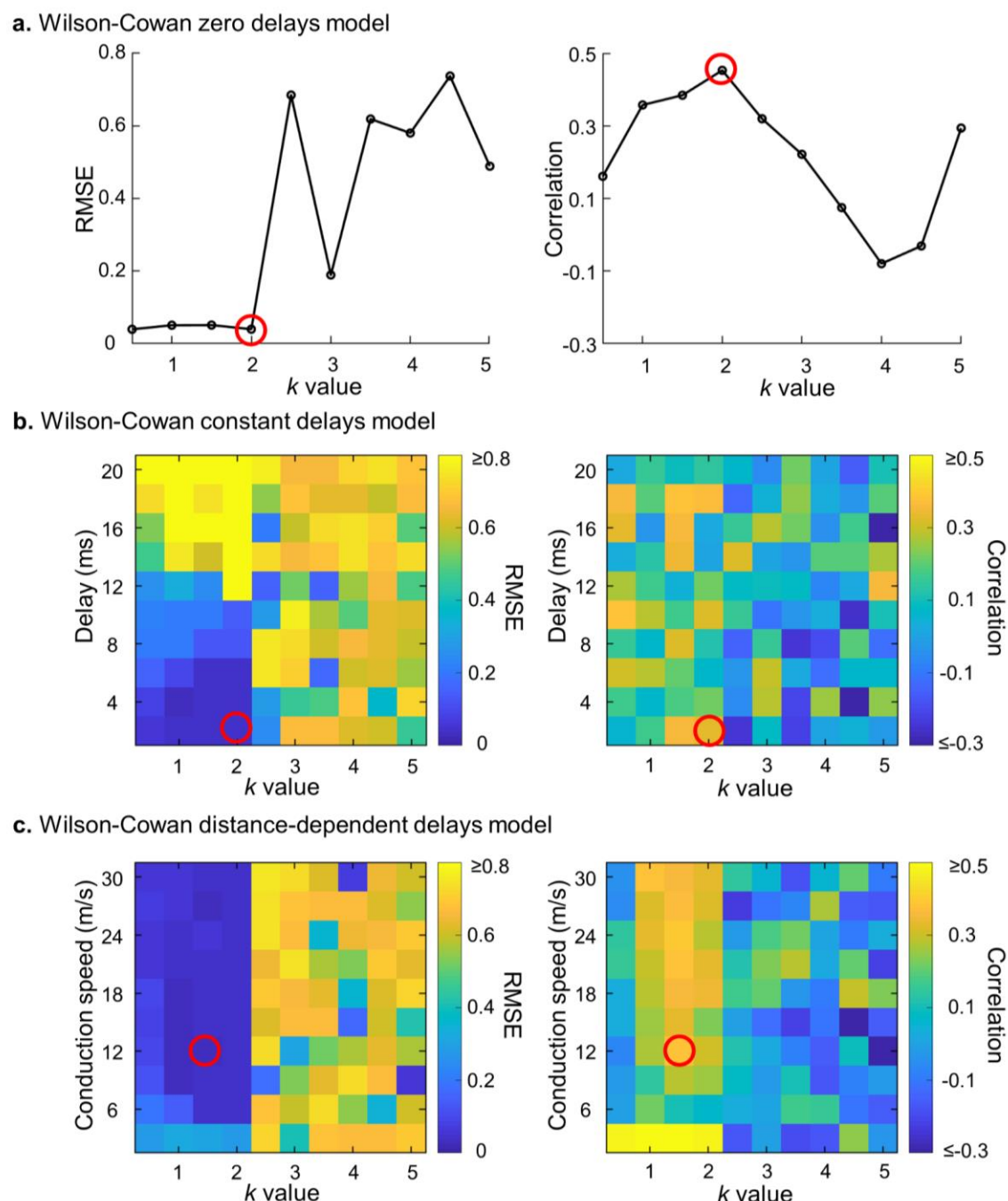576   synchronization, which we estimated as the average of 23 held out subject-level matrices.

Figure 2. Grid search for optimal parameter values of each model. a. RMSE and Correlation values for a range of k values, for Wilson-Cowan zero delays model b. RMSE and Correlation values for every combination of a range of k-values and a range of delay values, for Wilson-Cowan constant delays model c. RMSE and Correlation values for every combination of a range of k-values and range of conduction speed values, for Wilson-Cowan distance-dependent delays model. k is the scalar multiplier over the structural connectome.

586

3.2 Model comparison

We compared the Wilson-Cowan zero delays, Wilson-Cowan constant delays and Wilson-Cowan distance-dependent delays models. To do this, we compared the correspondences between their respective model-generated networks of phase-synchronization, and the testing set MEG-derived network of phase-synchronization. We quantified correspondence with RMSE and Correlation between upper triangular elements of the model-generated matrices from 20 simulations of each model and the testing set MEG-derived matrix. We used independent samples t-tests to compare performances between models and Cohen's d to measure effect sizes. RMSE values from the constant delays model (mean = 0.041) are higher than RMSE values from both the zero delays (mean = 0.039) (two-tailed $p = 1.1 \times 10^{-8}$, Cohen's $d = 2.3$) and distance-dependent delays models (mean = 0.039) (two-tailed $p = 7.4 \times 10^{-5}$, Cohen's $d = 1.4$) (Figure 3, left panel). In contrast, there is no difference between RMSE values from the zero delays and distance-dependent delays models (two-tailed $p > 0.001$, Cohen's $d = 0.37$). Similarly, Correlation values from the constant delays model (mean = 0.37) are lower than Correlation values from the zero delays (mean = 0.47) (two-tailed $p = 4.7 \times 10^{-10}$, Cohen's $d = 2.62$) and distance-dependent delays models (mean = 0.46) (two-tailed $p = 1.6 \times 10^{-10}$, Cohen's $d = 2.74$) (Figure 3, right panel), while there is no difference in Correlation values from the zero delays and distance-dependent delays models (two-tailed $p > 0.001$, Cohen's $d = 0.12$). These results suggest that the presence of delays in the Wilson-Cowan distance-dependent delays model does not improve the correspondence between model-generated and MEG-derived networks, compared to the correspondence obtained with the Wilson-Cowan zero delays model. Hence, we chose the more parsimonious model, *i.e.* the Wilson-Cowan zero delays model, for further investigation.
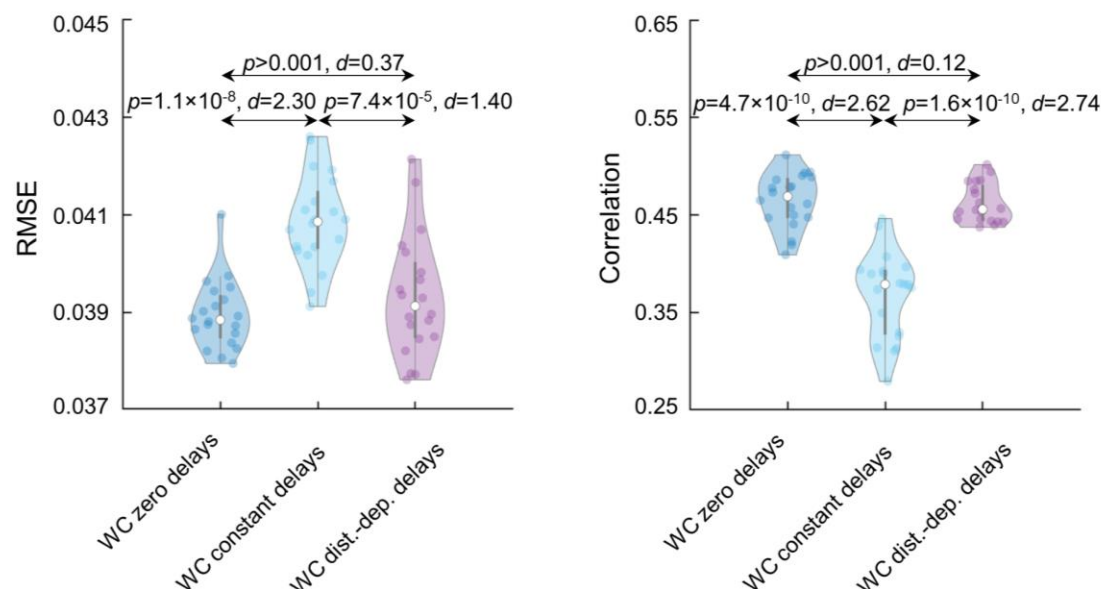
Figure 3. Including conduction delays does not improve model performance Violin plots of RMSE values for the Wilson-Cowan zero delays (mean = 0.039), constant delays (mean = 0.041) and distance-dependent delays models (mean = 0.039) (left panel). Violin plots of Correlation values for the Wilson-Cowan zero delays (mean = 0.47), constant delays (mean = 0.37) and distance-dependent delays models (mean = 0.46) (right panel).

3.3 Close correspondence between model-generated and MEG-derived network of phase-synchronization

We observed that the source-reconstructed dynamics of the Wilson-Cowan zero delays model exhibited intermittent dynamics (Figure 4a), also observed in MEG resting-state data (Shriki et al. (2013)). Further, the frequency spectrum of the dynamics displayed peaks in delta (1 - 4 Hz), alpha (8 - 12 Hz) and beta (12 - 30 Hz) frequency bands (Figure 4b), which have also been observed in MEG resting-state data (Mahjoory et al. (2020), Lopes da Silva (2013)).

We compared the levels of phase-synchronization within the source-reconstructed dynamics of the Wilson-Cowan zero delays model to those observed in source-reconstructed MEG resting-state data. To do this, we compared the mean of the Kuramoto order parameter (Breakspear et al. (2010)) of the source-reconstructed model dynamics and source-reconstructed MEG resting-state data, across participants in the held-out testing set. We observed mean of the Kuramoto order parameter of the model dynamics (Figure 4a) (mean = 8×10^{-2}, standard deviation = 9×10^{-3}) to be close to the mean of the Kuramoto order parameter of the source-reconstructed MEG resting-state data (mean = 8×10^{-2}, standard deviation = 1×10^{-2}). Hence, the source-

635 reconstructed dynamics of the Wilson-Cowan zero delays model display similar levels of

636 phase-synchronization as those observed in source-reconstructed MEG resting-state.
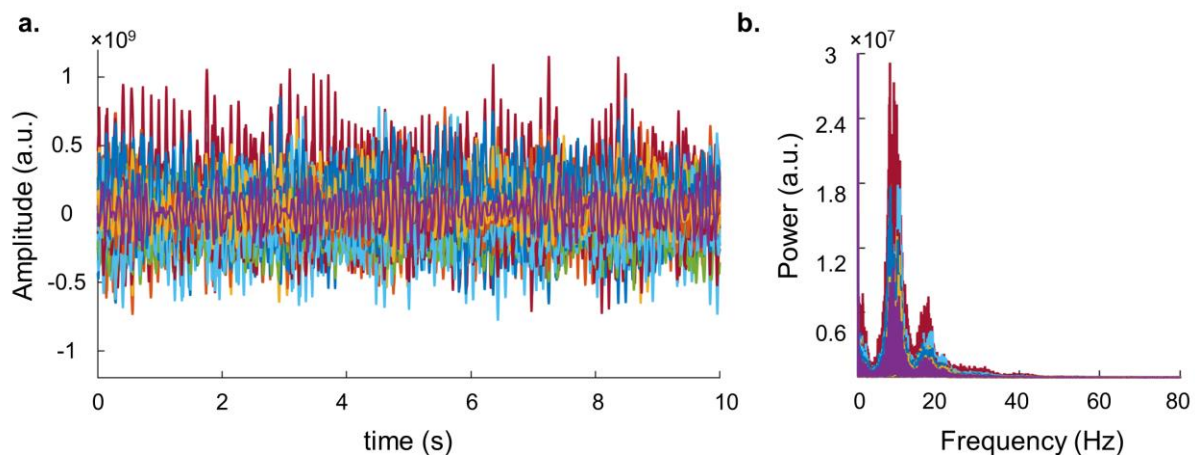

637

638 **Figure 4. Intermittent dynamics and peaks in the frequency spectrum of dynamics of**

639 **Wilson-Cowan zero delays model are similar to those observed in MEG resting-state.** a.

640 10-second time course of model dynamics from all brain regions for example subject b.

641 Frequency spectrum of model dynamics for 10-second segment of model dynamics from all

642 brain regions, for example subject. Different colours indicate time course/frequency spectrum

643 of different brain regions. Same colour in panels a, b belongs to the same brain region.

644

645 We next assessed the correspondence between the mean model-generated and MEG-derived

646 networks of phase-synchronization. The mean model-generated network was the average of 20

647 model-generated networks, each estimated from simulated model data from different initial

648 conditions. We compared the mean model-generated network of phase-synchronization to the

649 testing set MEG-derived network. Specifically, we compared the distributions of mean model-

650 generated and MEG-derived phase-synchronization values, and compared the RMSE and

651 Correlation between the mean model-generated and MEG-derived matrices against their

652 corresponding permutation-based null distributions. The distributions of mean model-

653 generated and MEG-derived phase-synchronization values are similar, with central tendency

654 (median = 0.09) and dispersion (median absolute deviation = 0.02) of mean model-generated

655 network values close to central tendency (median = 0.07) and dispersion (median absolute

656 deviation = 0.02) of MEG-derived network values (Figure 5a). RMSE = 0.04 between mean

657 model-generated and MEG-derived matrices is lower than chance ($z = $ -29.9, one-tailed $p = 6.7$

658 $\times 10^{-197}$), and Correlation = 0.49 between mean model-generated and MEG-derived networks

659 is higher than chance ($z = 25.4$, one-tailed $p = 0$) (Figure 5b,c). Further, most top 5 percentile

strongest connections lie within and between parietal, temporal and occipital regions, for both mean model-generated and MEG-derived networks of phase-synchronization (Figure 5d). Taken together, the results demonstrate a close correspondence between the mean model-generated and MEG-derived networks of phase-synchronization.
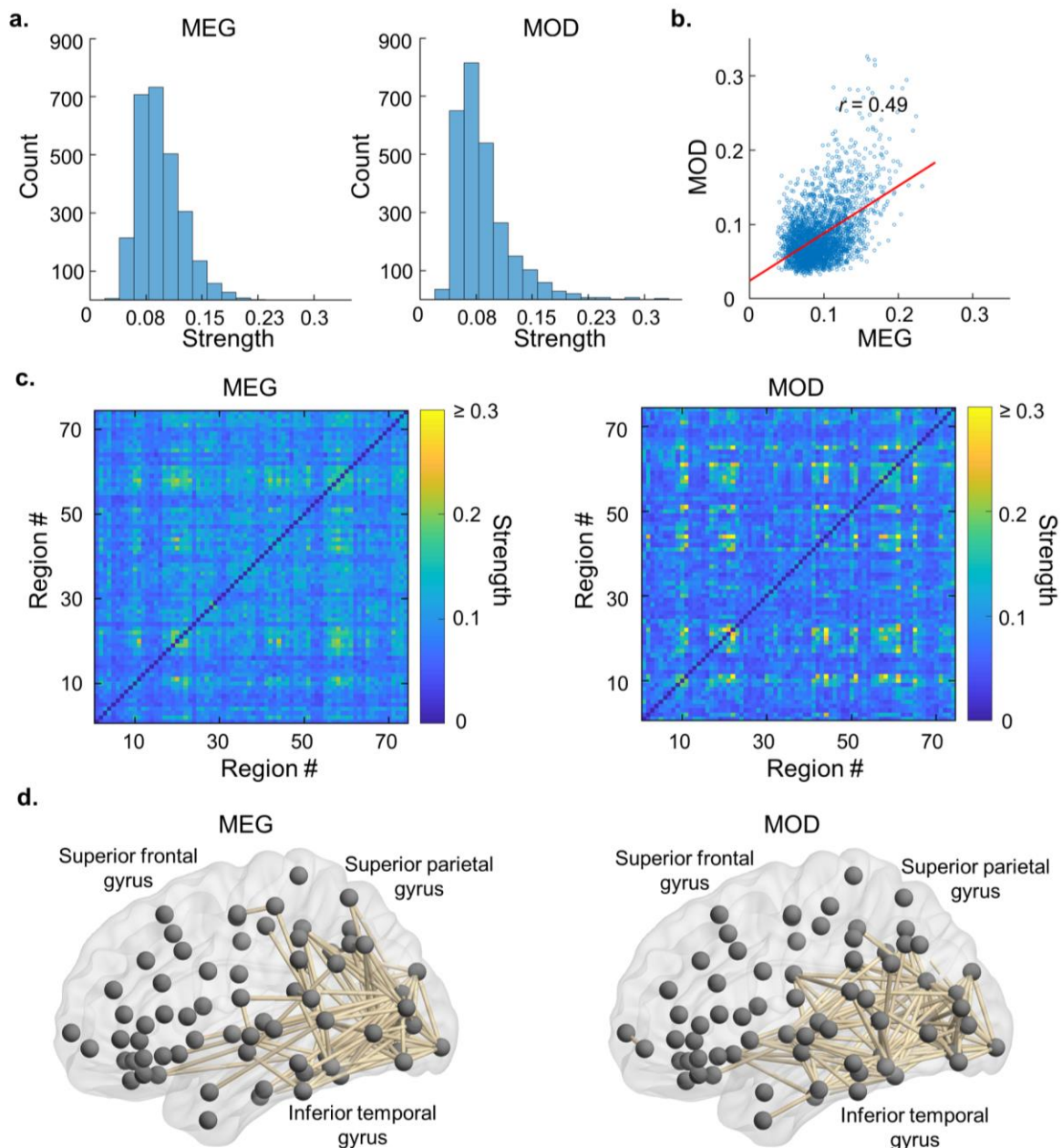

Figure 5. Close correspondence between mean model-generated network and MEG-derived network of phase-synchronization a. Histogram of connection strengths for mean model-generated and MEG-derived networks of phase-synchronization b. Scatter plot of connection strengths for MEG-derived network of phase-synchronization against mean model-generated network of phase-synchronization c. Matrices of connection strengths between every pair of brain regions for mean model-generated and MEG-derived network of phase-

671   synchronization. d. Brain network visualisation of top 5 percentile strongest connections for

672   mean model-generated and MEG-derived networks of phase-synchronization. MOD = model.

673   Brain networks were visualised with BrainNet Viewer (http://www.nitrc.org/projects/bnv/)

674   (Xia et al. (2013)).

675

676   We assessed the sensitivity of the Wilson-Cowan zero delays model, to changes in the values

677   of model parameters. To do this, we performed a sensitivity analysis wherein we estimated

678   change in model performance to small changes in the values of model parameters. We varied

679   the value of each non-zero parameter from -10% to 10% of its original value, while keeping all

680   other parameters at their original value. The RMSE and Correlation from simulating these

681   jittered models were z-scored against the 20 RMSE and Correlation values from simulating the

682   original model, to estimate the change in model performance. We found the model performance

683   to be robust to changes in values of k and w_{ii} parameters (z values < 3), *i.e.* the scalar multiplier

684   over the structural connectome and weight of self-inhibitory connections of Wilson-Cowan

685   oscillators respectively. However, the model performance is sensitive to changes in the values

686   of all other model parameters (z values > 3) (Figure S1). Hence, we observe that the Wilson-

687   Cowan zero delays model is sensitive to changes in the values of its model parameters.

688

689   We have shared the mean model-generated network and networks from each of 20 simulations

690   of the Wilson-Cowan zero delays model, through an open dataset (Williams et al. (2021b)).

691

692   **3.4 Determining features of each model component contributing to model performance**

693   The Wilson-Cowan zero delays model represents the hypothesis that the Wilson-Cowan

694   oscillatory dynamics interact with the pattern of structural connections to produce networks of

695   phase-synchronization corresponding to MEG-derived networks of phase-synchronization.

696   Hence, it postulates that both the pattern of structural connections and Wilson-Cowan

697   oscillatory dynamics contribute to the observed correspondence.

698

699   We tested the hypothesis that the pattern of structural connections contributes to the

700   correspondence between model-generated and MEG-derived networks. To do this, we

701   compared correspondence obtained with the original model against correspondence obtained

702   with null models containing degree-preserved randomised versions of the structural

703   connectome, all other aspects of the null model being identical to the original model. The

704   structural connectome from each of the null models had the same number of connections to

705   each brain region as the original structural connectome, but the pattern of connections between
706   regions was different from that of the original structural connectome. We used RMSE and
707   Correlation between the model-generated and testing set MEG-derived matrices to quantify
708   correspondence. Mean RMSE with the original model of 0.04 was lower (z = -3.7, one-tailed
709    $p = 1 \times 10^{-4}$) and mean Correlation of 0.47 was higher (z = 8.4, one-tailed $p = 0$) than the set of
710   RMSE and Correlation values yielded by null models containing degree-preserved randomised
711   versions of the original structural connectome (Figure 6a). These results confirm that the
712   pattern of connections in the structural connectome contributes to the observed correspondence
713   between model-generated and MEG-derived networks, over and above the number of
714   connections, *i.e.* degree, to each brain region.

715

716   Given the contribution of the pattern of connections of the structural connectome to the
717   observed correspondence between model-generated and MEG-derived networks, we
718   investigated if the model-generated network is merely a recapitulation of the structural
719   connectome. To do this, we compared Correlation between the model-generated matrix and the
720   testing set MEG-derived matrix, against Correlations between 100 bootstrapped versions of the
721   structural connectome matrix and the testing set MEG-derived matrix. Mean Correlation of
722   0.47 between the model-generated and MEG-derived matrices is higher (z = 181.5, one-tailed
723    $p = 0$) than Correlations between bootstrapped versions of the structural connectome matrix
724   and the MEG-derived matrix (Figure S2). These results demonstrate that the model does not
725   merely recapitulate the structural connectome at the level of its dynamics, but that it operates
726   on the structural connectome in a non-trivial way to produce the observed MEG-derived matrix
727   of phase-synchronization.

728

729   We tested the hypothesis that the Wilson-Cowan oscillatory dynamics contributes to the
730   comparison between model-generated and MEG-derived networks of phase-synchronization.
731   To do this, we compared correspondence obtained with the original model against
732   correspondence obtained with null models wherein the dynamics of each brain region were
733   described by random dynamics interacting through the structural connectome used in the
734   original model. The mean and range of random dynamics were matched to those of the Wilson-
735   Cowan oscillators. For the random node dynamics model also, we estimated the model
736   parameter $k,$ the scalar multiplier over the structural connectome, with the same procedure as
737   for the Wilson-Cowan zero delays model (Section 2.6). We used RMSE and Correlation
738   between the model-generated and testing set MEG-derived matrices to quantify

739   correspondence. Note that Correlation is insensitive to scale of the compared phase-
740   synchronization strengths, hence it would yield high values for similar patterns of model-
741   generated and MEG-derived phase-synchronization even if the random node dynamics model
742   produced weaker phase-synchronization strengths than those observed in the MEG-derived
743   networks. Just as for the Wilson-Cowan zero delays model, the optimal value of k for the
744   random node dynamics model was identified as 2. Mean RMSE with the original model of 0.04
745   was lower (z = -40.8, one-tailed p = 0) and mean Correlation of 0.47 was higher (z = 4.9, one-
746   tailed p = 5 × 10^{-7}) than the set of RMSE and Correlation values yielded by null models
747   containing random node dynamics instead of Wilson-Cowan oscillatory dynamics (Figure 6b).
748   These results confirm that the Wilson-Cowan oscillatory dynamics contributes to the observed
749   correspondence between model-generated and MEG-derived networks, over and above
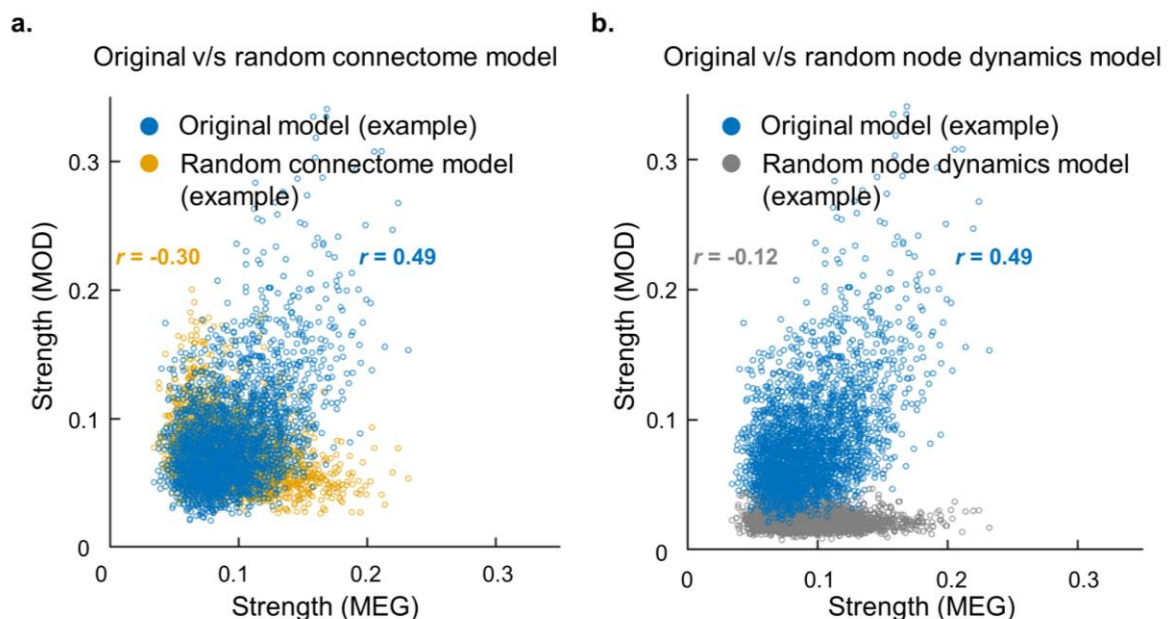750   dynamics with the same mean and range.

751

752   **Figure 6. The pattern of connections in the structural connectome and dynamics of**
753   **Wilson-Cowan oscillators, contribute to correspondence between model-generated and**
754   **MEG-derived networks of phase-synchronization** a. Scatter plot of connection strengths
755   from MEG-derived network and example model-generated network (blue) and of connection
756   strengths from MEG-derived network and example null model-generated network, wherein
757   structural connectome is randomised (yellow). b. Scatter plot of connection strengths from
758   MEG-derived network and example model-generated network (blue) and scatter plot of
759   connection strengths from MEG-derived network and null model-generated network, wherein
760   node dynamics are randomised (dark gray). MOD = model.

761

762 Given the contribution of Wilson-Cowan oscillator dynamics to the correspondence between
763 model-generated and MEG-derived networks, we investigated if the mere presence of
764 oscillatory rather than random node dynamics would produce the observed correspondence. To
765 do this, we compared correspondence obtained with the Wilson-Cowan zero delays model
766 against correspondence obtained with an equivalent Kuramoto oscillator model, which also
767 produces oscillatory dynamics. No statistically significant difference in the correspondences
768 with the Wilson-Cowan zero delays model and Kuramoto oscillator model would imply the
769 mere presence of oscillatory node dynamics produces a correspondence between model-
770 generated and MEG-derived networks. We quantified correspondence using the RMSE and
771 Correlation between the respective model-generated and MEG-derived matrices of phase-
772 synchronization. We identified $k = 0.5$ as the optimal value of the scalar multiplier over the
773 structural connectome for the Kuramoto oscillator model. Mean RMSE of 0.04 with the
774 Wilson-zero delays model was lower than mean RMSE of 0.53 with the Kuramoto oscillator
775 model (two-tailed $p = 8.4 \times 10^{-59}$). Similarly, mean Correlation of 0.47 with the Wilson-Cowan
776 zero delays model is higher than mean Correlation of 0.13 with the Kuramoto oscillator model
777 (two-tailed $p = 2.2 \times 10^{-37}$) (Figure S3). These results demonstrate the mere presence of
778 oscillatory node dynamics does not produce the observed correspondence between model-
779 generated and MEG-derived networks. Rather, it is the oscillatory dynamics of the Wilson-
780 Cowan oscillators resulting from the interaction between excitatory and inhibitory neuronal
781 populations, which produces the observed correspondence.

782

783 **3.5 Robustness of results**

784 Finally, we investigated the robustness of the obtained correspondence between model-
785 generated and MEG-derived networks, to choices made for the simulations and analyses. To
786 do this, we compared correspondence obtained with different solvers and with different relative
787 tolerance values for the model simulations. In addition, we determined if changing the modeled
788 hemisphere from left to right would qualitatively change the correspondence between the
789 model-generated and MEG-derived networks. We quantified correspondence by the RMSE
790 and Correlation between the model-generated and MEG-derived matrices of phase-
791 synchronization. We used the ODE45 solver in the original simulations, but RMSE and
792 Correlation values are not different when ODE23 and ODE113 solvers were used (two-tailed
793 $p > 0.001$ for each) (Figure 7a). Similarly, we used relative tolerance of 10^{-3} for the original
794 simulations, which yielded RMSE and Correlation values neither different to those obtained
795 with lower relative tolerance values of 10^{-4} and 10^{-5} nor a higher relative tolerance of 10^{-2} (two-

796   tailed $p > 0.001$ for each) (Figure 7b). Changing the modeled hemisphere from left to right
797   also yielded a moderate correspondence between the model-generated and MEG-derived
798   network (Correlation = 0.33) (Figure S4). Hence,   the correspondence between model-
799   generated and MEG-derived networks of phase-synchronization, were robust to choices made
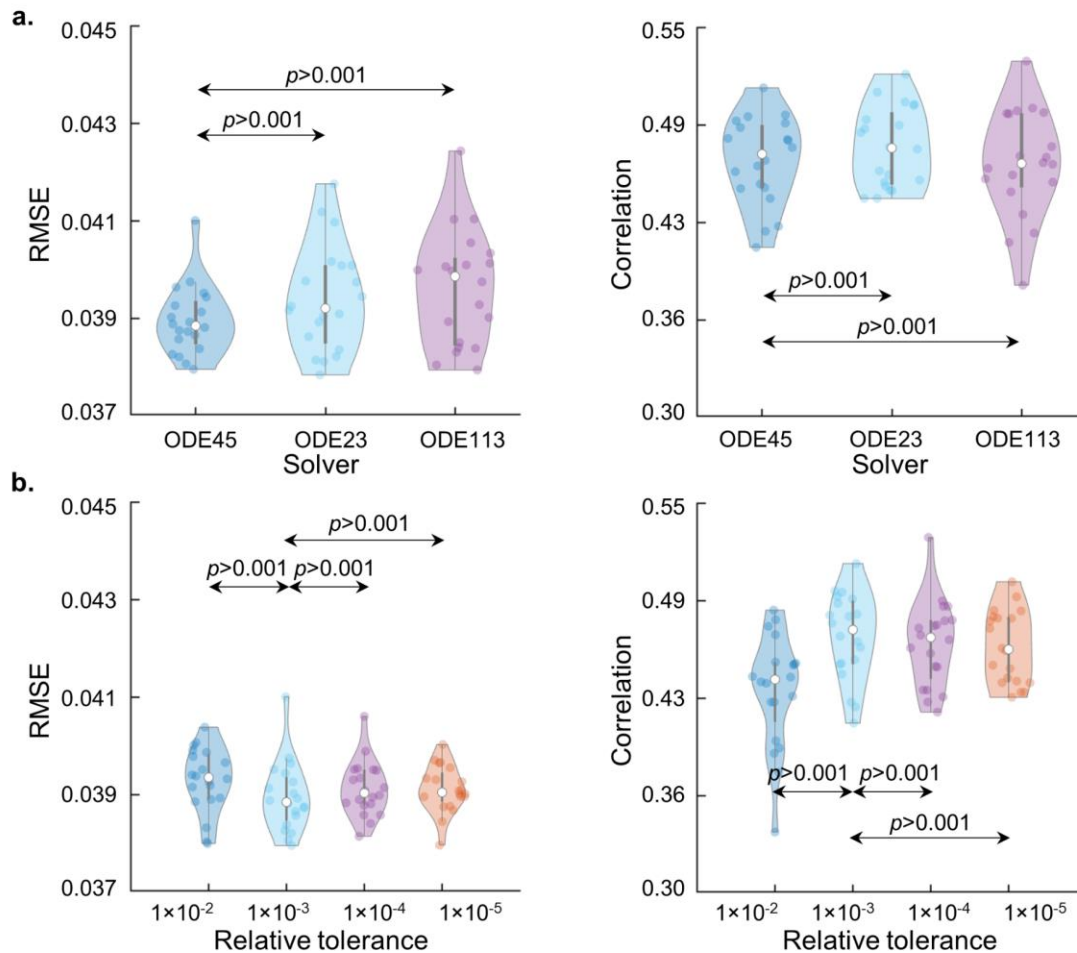800   for the simulations and analyses.

802   **Figure 7. Results are robust to changes in solver and relative tolerance of solution** a.
803   Boxplot of RMSE and Correlation with different solvers. Solver used in the original model was
804   ODE45. b. Boxplot of RMSE and Correlation at different relative tolerances of solution.
805   Relative tolerance used in the original model was 10^{-3}.

806 # 4. Discussion

807   Large-scale networks of phase-synchronization are widely observed with EEG or MEG during
808   rest and task. BNMs are used to produce model-generated networks corresponding to MEG-
809   derived networks of phase-synchronization, but the respective roles of conduction delays, the
810   structural connectome and dynamics of models of individual brain regions, in obtaining this

811   correspondence remain unknown. In this paper, we investigated the roles of conduction delays,

812   the structural connectome and dynamics of models of individual regions, in producing

813   networks of phase-synchronization corresponding to those observed in MEG resting-state. We

814   found no evidence that including conduction delays improves the correspondence between the

815   model-generated and MEG-derived networks of phase-synchronization. Further, we

816   demonstrated that both the pattern of structural connections and Wilson-Cowan oscillatory

817   dynamics contribute to obtaining the observed correspondence between model-generated and

818   MEG-derived networks of phase-synchronization.

819

820   The topological organisation of the structural connectome, *i.e.,* its pattern of connections,

821   contributes to the observed correspondence between the model-generated and MEG-derived

822   network of phase-synchronization. Previous studies have used the structural connectome within

823   BNMs to produce other phenomena, such as networks matching experimentally observed

824   fMRI-derived networks (Deco et al. (2009)), MEG-derived networks of amplitude correlation

825   (Tewarie et al. (2019)) and spatial distribution of oscillation amplitudes observed in MEG

826   resting-state (Raj et al. (2019)). Studies have also used the structural connectome in models to

827   produce networks matching MEG-derived networks of phase-synchronization, but these have

828   been via abstract statistical or oscillator models (Finger et al. (2016)), graph theory measures

829   (Wodeyar & Srinivasan (2019)) or formal series expansions (Meier et al. (2016)). A single

830   study used the structural connectome with a biologically plausible model to produce networks

831   of phase-synchronization matching those observed in the MEG resting-state (Abeysuriya et al.

832   (2018)). Our study advances findings from these studies in the following ways: 1.) We used

833   comparison against null models to identify the specific feature of the structural connectome,

834   *i.e.,* its topological organisation, rather than lower-level properties such as the degree of each

835   brain region, contributing to the observed correspondence between model-generated and MEG-

836   derived networks of phase-synchronization, and 2.) We demonstrated that the correspondence

837   between the model-generated and MEG-derived networks of phase-synchronization is not

838   explained merely by the correspondence between the structural connectome and the MEG-

839   derived network of phase-synchronization. Consistent with computational modelling on the

840   relationship between the structural connectome and networks of phase-synchronization

841   (Forrester et al. (2020)), these results suggest a significant but nontrivial relationship between

842   the structural connectome and the model-generated network of phase-synchronization.

843

844 The dynamics of Wilson-Cowan oscillators contribute to the observed correspondence between
845 model-generated and MEG-derived networks of phase-synchronization. Previous modelling
846 studies have studied the role of the structural connectome in producing observed functional
847 networks, but the role of dynamics of brain regions in producing these networks has not
848 received much attention. A recent computational modelling study (Forrester et al. (2020))
849 demonstrated the influence of node dynamics on the relationship between the structural
850 connectome and model-generated networks of phase-synchronization. The study demonstrated
851 that oscillatory node dynamics are accompanied by a nontrivial relationship between the
852 structural connectome and model-generated networks of phase-synchronization. Our study
853 advances previous work in the following ways: 1.) While previous work has related oscillatory
854 node dynamics to model-generated networks, this is the first work demonstrating the
855 importance of oscillatory node dynamics in producing networks of phase-synchronization
856 corresponding to those observed in experimental MEG resting-state. 2.) We illustrate the
857 importance of specifically Wilson-Cowan oscillatory dynamics, by demonstrating that the
858 Wilson-Cowan zero delays model produces networks with closer correspondence to MEG-
859 derived networks of phase-synchronization than does an equivalent model of Kuramoto
860 oscillators. This result is consistent with computational modelling demonstrating the influence
861 of both amplitude and phase dynamics, as produced by Wilson-Cowan oscillators, on estimates
862 of phase-synchronization (Daffertshofer & van Wijk (2011)). Kuramoto oscillators only yield
863 descriptions of phase dynamics. Hence, the oscillatory dynamics resulting from the interaction
864 between excitatory and inhibitory neuronal populations, as described by Wilson-Cowan
865 oscillators, contributes to producing networks of phase-synchronization corresponding to those
866 observed in MEG resting-state.

867

868 We find no evidence that including conduction delays improves the correspondence between
869 model-generated and MEG-derived networks of phase-synchronization. Modelling studies
870 investigating the role of delays in producing networks resembling fMRI-derived functional
871 networks or MEG-derived networks of amplitude correlation have yielded differing results.
872 Results of some studies suggest the importance of delays in producing fMRI-derived networks
873 (Ghosh et al. (2008), Deco et al. (2009)) or MEG-derived networks of amplitude correlation
874 (Cabral et al. (2014), Nakagawa et al. (2014)), while other modelling studies not including
875 delays also produce networks resembling fMRI-derived (Honey et al. (2007)) or MEG-derived
876 networks of amplitude correlation (Deco et al. (2017)). The role of conduction delays in
877 producing networks resembling MEG-derived networks of phase-synchronization has not

878   received much attention. A recent modelling study (Abeysuriya et al. (2018)) reported that, in

879   the special case of a high mean activity level (mean activity = 0.3) of Wilson-Cowan oscillators

880   imposed by synaptic plasticity mechanisms, conduction delays were not necessary to producing

881   networks resembling MEG-derived networks of phase-synchronization. In our study, we

882   advance previous work by demonstrating that, also in the more general case of no specific mean

883   target activity imposed by synaptic plasticity mechanisms, a close correspondence between

884   model-generated and MEG-derived networks of phase-synchronization can be achieved.

885

886   The absence of evidence in our study, for the role of delays in producing MEG-derived

887   networks of phase-synchronization, might be either due to errors in the estimates of conduction

888   delay or due to conduction delays not being mechanistically important in producing MEG-

889   derived networks of phase-synchronization. If the latter were true, one would expect the

890   Wilson-Cowan constant delays and Wilson-Cowan distance-dependent delays model to

891   produce networks corresponding equally to the MEG-derived network of phase-

892   synchronization. However, the Wilson-Cowan distance-dependent delays model produces

893   networks correspondingly more closely to the MEG-derived network, than networks produced

894   by the Wilson-Cowan constant delays model. In fact, the Wilson-Cowan distance-dependent

895   delays model produces networks corresponding as closely to the MEG-derived network, as

896   networks produced by the Wilson-Cowan zero delays model. Hence, we propose that improved

897   accuracy in estimating conduction delays, by accounting for axonal diameter and myelination

898   (Nakagawa et al. (2014), Waxman & Swadlow (1977)) in addition to distance, could yield

899   improved correspondence between networks produced by the Wilson-Cowan distance-

900   dependent delays model and the MEG-derived network of phase-synchronization. Specialised

901   diffusion MRI sequences could yield estimates of myelination and axonal diameter (Drobnjak

902   et al. (2016), Whittall et al. (1997)), but these estimates remain elusive.

903

904   The Wilson-Cowan zero delays model compares well to previously proposed BNMs producing

905   networks of phase-synchronization observed in the MEG resting-state. A strength of a recently

906   proposed BNM (Abeysuriya et al. (2018)) with distance-dependent conduction delays and

907   inhibitory synaptic plasticity, was that it used the same set of parameter values to

908   simultaneously produce a correspondence to both MEG-derived networks of amplitude

909   correlation and MEG-derived networks of phase-synchronization. However, two notable

910   aspects of the Wilson-Cowan zero delays model we propose are 1.) its parsimonious nature in

911   not including conduction delays or synaptic plasticity mechanisms, while still producing

912 networks corresponding closely ($\rho = 0.49$) to MEG-derived networks of phase-synchronization
913 and 2.) its strengths of phase-synchronization between regions were of the same order of
914 magnitude and closer to those observed in the MEG-derived network (RMSE = 0.04) compared
915 to previously proposed BNMs. However, a direct comparison between our model and those
916 used in previous studies is difficult due to differences in the brain parcellation atlases used,
917 number of hemispheres considered, measures of phase-synchronization used, as well as
918 processing details of MEG and model-generated data.

919

920 A limitation of the Wilson-Cowan zero delays model we propose is that while it does produce
921 networks corresponding to MEG-derived networks of phase-synchronization, it does not
922 simultaneously produce networks of amplitude correlation nor produce spatial distribution of
923 oscillation amplitudes corresponding to those observed in MEG resting-state (results not
924 shown). However, we did find these phenomena were produced by the model operating at very
925 low levels of structural coupling between regions, *e.g.,* k values of 10^{-3}, where k is the scalar
926 multiplier across the structural connectome. This was outside the range of structural coupling
927 strengths investigated in our study. Future studies will use likelihood-free inference methods
928 to estimate parameters from wider parameter ranges (Lintusaari et al. (2017), Lintusaari et al.
929 (2018), Gutmann & Corander (2016), Cranmer et al. (2020)). Sensitivity analysis of our model
930 revealed the model performance to be highly sensitive to values of model parameters. This
931 could be due to the absence, in the model, of empirically observed homeostatic mechanisms to
932 counteract the effect of changes in *e.g.,* the mean activity level of the Wilson-Cowan oscillators.

933

934 Future work could extend the model to include empirically observed spatial gradients in
935 synaptic excitation (Wang (2020)), which in turn produce empirically observed spatial
936 gradients in peak frequency (Hadida et al. (2019), Mahjoory et al. (2020)). The model could
937 also be extended to include the effects of noise (Faisal et al. (2008)), which has been suggested
938 to play a role in generating dynamics of resting-state data from other methodologies (Deco et
939 al. (2009)). These models, fit to MEG resting-state data, could be locally perturbed to emulate
940 task-related dynamics (Tiesinga et al. (2010)). Such virtual experiments could be used to
941 develop, test and refine hypotheses on biophysical substrates underlying observed networks of
942 phase-synchronization in MEG task data.

5. Conclusion

943

944 In this study, we investigated the respective contributions of conduction delays, the structural
945 connectome and dynamics of models of individual brain regions, in producing model-generated
946 networks of phase-synchronization corresponding to those observed in MEG resting-state.
947 Based on our investigations, we report no evidence for the role of conduction delays in
948 producing networks corresponding to MEG-derived networks of phase-synchronization.
949 Further, we demonstrate the contribution of the topological organisation of the structural
950 connectome and the dynamics of Wilson-Cowan oscillators in producing model-generated
951 networks of phase-synchronization that correspond to those observed in MEG resting-state.
952 Future studies will extend these models and subject them to local perturbations to provide
953 insight on biophysical substrates underlying observed networks in rest and task conditions.

Acknowledgements

954

References

962

963 1. Abeysuriya R., Hadida J., Sotiropoulus S., Jbabdi S., Becker R., Hunt B., Brookes M.,
964   Woolrich M. (2018) A biophysical model of dynamic balancing of excitation and
965   inhibition in fast oscillatory large-scale networks. *PLoS Comput Biol*, 14(2): e1006007
966 2. Beckmann C., DeLuca M., Devlin J., Smith S. (2005) Investigations into resting-state
967   connectivity using independent component analysis. *Philos Trans R Soc Lond B Biol
968   Sci,* 360(1457): 1001-1013
969 3. Binzegger T., Douglas R., Martin K. (2004) A quantitative map of the circuit of the cat
970   primary visual cortex. *J Neurosci*, 24(39): 8441-8453

4. Bogacki P., Shampine L. (1996) An efficient Runge-Kutta (4,5) pair. *Comput Math with Appl*, 32(6): 15-28

5. Breakspear M., Heitmann S., Daffertshofer, A. (2010) Generative models of cortical oscillations: neurobiological implications of the Kuramoto model. *Front Hum Neurosci*, 4, 190

6. Brookes M., Woolrich M., Barnes G. (2012) Measuring functional connectivity in MEG: a multivariate approach insensitive to linear source leakage. *NeuroImage*, 63(2): 910-920

7. Cabral J., Luckhoo H., Woolrich M., Joensson M., Mohseni H., Baker A., Kringelbach M., Deco G. (2014) Exploring mechanisms of spontaneous functional connectivity in MEG: how delayed network interactions lead to structured amplitude envelopes of band-pass filtered oscillations. *NeuroImage*, 90: 423-435.

8. Cohen J. (1988) Statistical Power Analysis for the Behavioural Sciences. New York, NY: Routledge Academic

9. Cohen J., D'Esposito M. (2016) The segregation and integration of distinct brain networks and their relationship to cognition. *J Neurosci*, 36(48): 12083-12094

10. Colclough G., Brookes M., Smith S., Woolrich M. (2015) A symmetric multivariate leakage correction for MEG connectomes. *NeuroImage*, 117: 439-448

11. Cole M., Reynolds J., Power J., Repovs G., Anticevic A., Braver T. (2013) Multi-task connectivity reveals flexible hubs for adaptive task control. *Nat Neurosci*, 16(9): 1348-1355

12. Cowan J., Neuman J., van Drongelen W. (2016) Wilson-Cowan equations for neocortical dynamics. *J Math Neurosci* 6, 1

13. Cranmer K., Brehmer J., Louppe G. (2020) The frontier of simulation-based inference. *Proc Natl Acad Sci USA*, 117(48): 30055-30062

14. da Silva F. (2013) EEG and MEG: Relevance to Neuroscience. *Neuron*, 80(5): 1112-1128

15. Daffertshofer A., van Wijk B. (2011) On the influence of amplitude on the connectivity between phases. *Front NeuroInform.* 5:6

16. Damoiseaux J., Rombouts S., Barkhof F., Scheltens P., Stam C., Smith S., Beckmann C. (2006) Consistent resting-state networks across healthy subjects. *Proc Natl Acad Sci USA*, 103(37): 13848-13853

17. Deco G., Cabral J., Woolrich M., Stevner A., Van Hartevelt T., Kringelbach M. (2017) Single or multiple frequency generators in on-going brain activity: a mechanistic whole-brain model of empirical MEG data. *NeuroImage*, 152: 538-550

18. Deco G., Jirsa V., McIntosh A., Sporns O., Kötter R. (2009) Key role of coupling, delay and noise in resting brain fluctuations. *Proc Natl Acad Sci USA*, 106(25): 10302-10307

19. Deco G., Tononi G., Boly M., Kringelbach M. (2015) Rethinking segregation and integration: contributions of whole-brain modelling. *Nat Rev Neurosci*, 16(7): 430-439

20. Destrieux C., Fischl B., Dale A., Halgren E. (2010) Automatic parcellation of human cortical gyri and sulci using standard anatomical nomenclature. *NeuroImage*, 53(1): 1-15

21. Douglas R. Martin K., Whitteridge D. (1989) A canonical microcircuit for neocortex. *Neural Comput*, 1(4): 480-488

22. Drobnjak I., Zhang H., Ianus A., Kaden E., Alexander D. (2016) PGSE, OGSE and sensitivity to axon diameter in diffusion MRI: insight from a simulation study. *Magn Reson Med*, 75(2): 688-700

23. Faisal A., Selen L., Wolpert D. (2008) Noise in the nervous system. *Nat Rev Neurosci*, 9(4): 292-303

24. Finger H., Bönstrup M., Cheng B., Messé A., Hilgetag C., Thomalla G., Gerloff C., König P. (2016) Modeling of large-scale functional brain networks based on structural connectivity from DTI: comparison with EEG derived phase coupling networks and evaluation of alternative methods along the modeling path. *PLoS Comput Biol*, 12(8): e1005025

25. Forrester M., Crofts J., Sotiropoulos S., Coombes S., O'Dea R. (2020) The role of node dynamics in shaping emergent functional connectivity patterns in the brain. *Netw Neurosci*, 4(2): 467-483

26. Fries P. (2005) A mechanism for cognitive dynamics: neuronal communication through neuronal coherence. *Trends Cogn Sci,* 9(10): 474-480.

27. Ghosh A., Rho Y., McIntosh A., Kötter R., Jirsa V. (2008) Cortical network dynamics with time delays reveals functional connectivity in the resting brain. *Cogn Neurodyn,* 2(2): 115-120

28. Gutmann M., Coriander J. (2016) Bayesian optimization for likelihood-free inference of simulator-based statistical models. *J Mach Learn Res*, 17: 1-47

29. Hadida J., Sotiropoulos S., Abeysuriya R., Woolrich M., Jbabdi S. (2018) Bayesian optimisation of large-scale biophysical networks. *NeuroImage* 174: 219-236

30. Hadida J., Sotiropoulos S., Jbabdi S., Woolrich M. (2019) Capturing MEG spectral dynamics with non-uniform biophysical networks. Poster presented at: 25th Annual Meeting of the Organization for Human Brain Mapping (OHBM) 2019, June 9-13 2019, Rome, Italy

31. Hämäläinen M., Ilmoniemi R. (1994) Interpreting fields of the brain: minimum-norm estimates. *Med Biol Eng Comput* 32: 35-42

32. Heitmann S., Auburn M., Breakspear M. (2018) The Brain Dynamics Toolbox for MATLAB. *Neurocomputing*, 315: 82-88

33. Hipp J., Hawelleck D., Corbetta M., Siegel M, Engel A. (2012) Large-scale cortical correlation structure of spontaneous oscillatory activity. *Nat Neurosci*, 15(6): 884-890

34. Hirvonen J., Monto S., Wang S., Palva M., Palva S. (2018) Dynamic large-scale network synchronization from perception to action. *Netw Neurosci*, 2(4): 442-463

35. Hlinka J., Coombes S. (2012) Using computational models to relate structural and functional brain connectivity. *Eur J Neurosci*, 36(2): 2137-2145

36. Honey C., Kötter R., Breakspear M., Sporns O. (2007) Network structure of the cerebral cortex shapes functional connectivity on multiple time scales. *Proc Natl Acad Sci USA,* 104(24): 10240–10245

37. Jansen B., Rit V. (1995) Electroencephalogram and visual evoked potential generation in a mathematical model of coupled cortical columns. *Biol Cybern*, 73: 357-366

38. Kilpatrick Z. (2013) Wilson-Cowan model. *In: Encyclopedia of Computational Neuroscience*, edited by Jaeger D., Jung R. New York: Springer, 1-5

39. Kitzbichler M., Henson R., Smith M., Nathan P., Bullmore E. (2011) Cognitive effort drives workspace configuration of human brain functional networks. *J Neurosci*, 31(22): 8259-8270

40. Korhonen O., Palva S., Palva M. (2014) Sparse weightings for collapsing inverse solutions to cortical parcellations optimize M/EEG source reconstruction accuracy. *J Neurosci Methods*, 226, 147-160

41. Kuramoto Y. (1984) Chemical Oscillations, Waves and Turbulence. *Mineola, NY: Dover Publications*.

42. Lintusaari J., Gutmann M., Dutta R., Kaski S., Corander J. (2017) Fundamentals and recent developments in Approximate Bayesian Computation. *Syst Biol*, 66(1): e66-e82

43. Lintusaari J., Vuollekoski H., Kangasraasio A., Skytén K., Jarvenpaa M., Marttinen P., Gutmann M., Vehtari A., Coriander J., Kaski S. (2018) ELFI: Engine for Likelihood-Free Inference. *J Mach Learn Res*, 19(16): 1-7

44. Lobier M., Palva M., Palva S. (2018) High-alpha band synchronization across frontal, parietal and visual cortex mediates behavioural and neuronal effects of visuospatial attention. *NeuroImage*, 165: 222-237

45. Mahjoory K., Schoffelen J-M., Keitel A., Gross J. (2020) The frequency gradient of human resting-state oscillations follow cortical hierarchies. *eLife* 9:e53715

46. Marzetti L., Basti A., Chella F., D'Andrea A., Syrjälä J., Pizzella V. (2019) Brain functional connectivity through phase coupling of neuronal oscillations: a perspective from magnetoencephalography. *Front. Neurosci*, 13, 964

47. Maslov S., Sneppen K. (2002) Specificity and stability in topology of protein networks. *Science*, 296(5569): 910-913

48. Meier J., Tewarie P., Hillebrand A., Douw L., van Dijk B., Stufflebeam S., Van Miegham P. (2016) A mapping between structural and functional brain networks. *Brain Connect*, 6(4): 298-311

49. Nakagawa T., Woolrich M., Luckhoo H., Joensson M, Mohseni H., Kringelbach M., Jirsa V., Deco G. (2014) How delays matter in an oscillatory whole-brain spiking-neuron network model for MEG alpha-rhythms at rest. *NeuroImage*, 87: 383-394.

50. Noori R., Park D., Griffiths J., Bells S., Frankland P., Mabbott D., Lefebvre J. (2020) Activity-dependent myelination: a glial mechanism of oscillatory self-organization in large-scale brain networks. *Proc Natl Acad Sci USA*, 117(24): 13227-13237

51. Oostenveld R., Fries P., Maris E., Schoffelen J-M. (2011) FieldTrip: Open source software for advanced analysis of MEG, EEG and invasive electrophysiological data. *Comput Intell Neurosci* 2011(1): 156869

52. Palva M., Monto S., Kulashekhar S., Palva S. (2010) Neuronal synchrony reveals working memory networks and predicts individual memory capacity. *Proc Natl Acad Sci USA*, 107(16): 7580-7585

53. Palva M., Palva S., Kaila K. (2005) Phase synchrony among neuronal oscillations in the human cortex. *Journal of Neuroscience*, 25 (15) 3962-3972

54. Palva M., Wang S., Palva S., Zhigalov A., Monto S., Brookes M., Schoffelen J., Jerbi K. (2018) Ghost interactions in MEG/EEG source space: A note of caution on inter-areal coupling measures. *NeuroImage*, 173: 632-643

55. Palva S., Palva M. (2012) Discovering oscillatory interaction networks with M/EEG: challenges and breakthroughs. *Trends Cogn Sci*, 16(4): 219-230

56. Pfeiffer C., Andersen L., Lundqvist D., Hämäläinen M., Schneiderman J., Oostenveld R. (2018) Localizing on-scalp MEG sensors using an array of magnetic dipole coils. *PLoS ONE* 13(5): e0191111

57. Raj A., Cai C., Xie X., Palacios E., Owen J., Mukherjee P., Nagarajan S. (2020) Spectral graph theory of brain oscillations. *Hum Brain Mapp*, 41(11): 2980-2998

58. Shampine L., Thompson S. (2001) Solving DDEs in MATLAB. *Appl Numer Math*, 37(4): 441-458

59. Shriki O., Alstott J., Carver F., Holroyd T., Henson R., Smith M., Coppola R., Bullmore E., Plenz D. (2013) Neuronal avalanches in the resting MEG of the human brain. *Journal Neurosci.* 33(16): 7079-7090

60. Siebenhühner F., Wang S., Arnulfo G., Lampinen A., Nobili L., Palva M., Palva S. (2020) Genuine cross-frequency coupling networks in human resting-state electrophysiological recordings. *PLoS Biol*, 18(5): e3000685

61. Siegel M., Donner T., Engel A. Spectral fingerprints of large-scale neuronal interactions. *Nat Rev Neurosci*, 13(2): 121-134

62. Singer W. (1999) Neuronal synchrony: a versatile code for definition of relations? *Neuron*, 24(1): 49-65

63. Singh R., Menon S., Sinha S. (2016) Complex patterns arise through spontaneous symmetry breaking in dense homogeneous networks of neural oscillators. *Sci Rep* 6(1): 1-8

64. Smith R., Tournier J., Calamante F., Connelly A. (2012) Anatomically-constrained tractography: improved diffusion MRI streamlines tractography through effective use of anatomical information. *NeuroImage*, 62(3): 1924-1938

65. Smith R., Tournier J., Calamante F., Connelly A. (2013) SIFT: Spherical-deconvolution informed filtering of tractograms. *NeuroImage*, 67: 298-312

66. Sreenivasan V., Menon S., Sinha S. (2017) Emergence of coupling-induced oscillations and broken symmetries in heterogenously driven nonlinear reaction networks. *Sci Rep* 7(1): 1-8

67. Taulu S., Hari R. (2009) Removal of magnetoencephalographic artifacts with temporal signal-space separation: demonstration with single-trial auditory-evoked responses. *Hum Brain Mapp*, 30: 1524-1534

68. Tewarie P., Abeysuriya R., Byrne Á., O'Neill G., Sotiropoulos S., Brookes M., Coombes S. (2019) How do spatially distinct frequency specific MEG networks emerge

1136   from one underlying structural connectome? The role of structural eigenmodes.
1137   *NeuroImage*, 186: 211-220

1138   69. Tiesinga P., Sejnowski T. (2010) Mechanisms for phase shifting in cortical networks
1139   and their role in communication through coherence. *Front Hum Neurosci*, 4, 196

1140   70. Traub R., Jefferys J., Whittington M. (1997) Simulation of gamma rhythms in networks
1141   of interneurons and pyramidal cells. *J Comput Neurosci* 4(2): 141-150

1142   71. Van Essen D., Smith S., Barch D., Behrens T., Yacoub E., Ugurbil K., WU-Minn HCP
1143   Consortium (2013) The WU-Minn Human Connectome Project: an overview.
1144   *NeuroImage*, 80: 62-79

1145   72. Vinck M., Oostenveld R., Wingerden M., Battaglia F., Pennartz C. (2011) An improved
1146   index of phase-synchronization for electrophysiological data in the presence of volume-
1147   conduction, noise and sample-size bias. *NeuroImage*, 55(4): 1548-1565

1148   73. Wang X-J. (2020) Macroscopic gradients of synaptic excitation and inhibition in the
1149   neocortex. *Nat Rev Neurosci*, 21: 169-178

1150   74. Waxman S., Swadlow H. (1977) The conduction properties of axons in central white
1151   matter. *Prog Neurobiol*, 8(4): 297-324

1152   75. Whittall K., Mackay A., Graeb D., Nugent R., Li D., Paty D. (1997) *In vivo*
1153   measurement of T_2 distributions and water contents in normal human brain. *Magn*
1154   *Reson Med*, 37(1): 34-43

1155   76. Williams (2021a, May 28). MATLAB implementations of networks of Wilson-
1156   Cowan oscillators with delayed interactions (Version 1). Zenodo.
1157   http://doi.org/10.5281/zenodo.4817655

1158   77. Williams N., Toselli B., Siebenhühner F., Palva S., Arnulfo G., Kaski S. Palva M.
1159   (2021b), "Connectomes of phase-synchronization generated by Wilson-Cowan
1160   network model", Mendeley Data, V1, doi: 10.17632/bgs7w9z24h.1

1161   78. Wilson H., Cowan J. (1972) Excitatory and inhibitory interactions in localized
1162   populations of model neurons. *Biophys J*, 12(1): 1-24

1163   79. Wodeyar A., Srinivasan R. (2019) Contribution of structural connectivity to MEG
1164   functional connectivity. *biorxiv*, 785600

1165   80. Woolrich M., Stephan K. (2013) Biophysical network models and the human
1166   connectome. *NeuroImage*, 80: 330-338.

1167   81. Xia M., Wang J., He Y. (2013) BrainNet Viewer: A network visualization tool for
1168   human brain connectomics. *PLoS ONE*, 8: e68910

1169   82. Zhigalov A., Arnulfo G., Nobili L., Palva S., Palva M. (2015) Relationship of fast-and-
1170   slow-timescale neuronal dynamics in human MEG and SEEG. *J Neurosci*, 35(13):
1171   5385-5396

1172   83. Zhigalov A., Arnulfo G., Nobili L., Palva S., Palva M. (2017) Modular co-organization
1173   of functional connectivity and scale-free dynamics in the human brain. *Netw Neurosci*
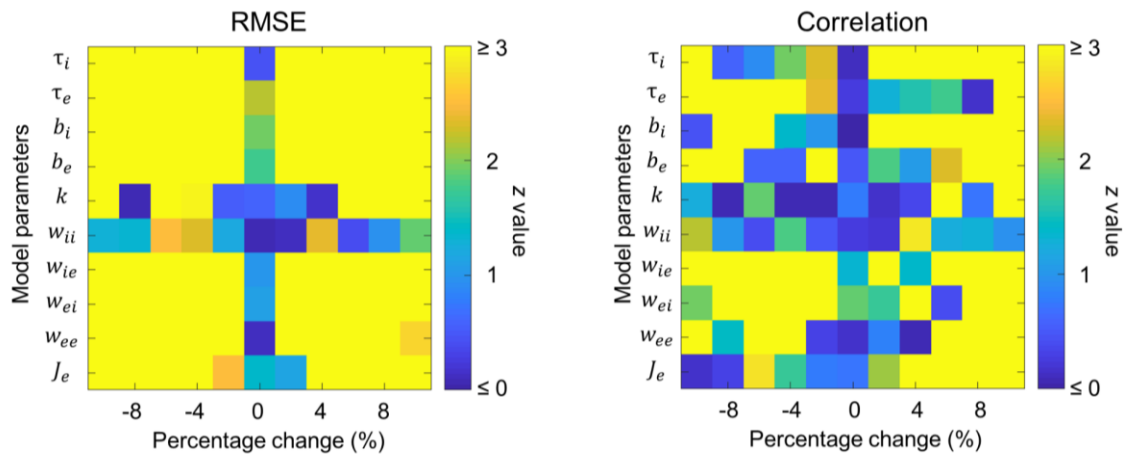1174   1(2):143-165

1175

1176

1177

1178

1179

1180

1181

1182

1183

1184

1185

1186

Supplementary figures

1187

1188

1189 **Figure S1. Model performance is sensitive to values of model parameters** Change in model
1190 performance, as measured by z-scored RMSE and z-scored Correlation, for percentage change
1191 in original value of each model parameter while keeping all other parameters at their original
1192 values.

1193

1194

1195

1196

1197

1198

Comparison of Structural and MEG-derived networks
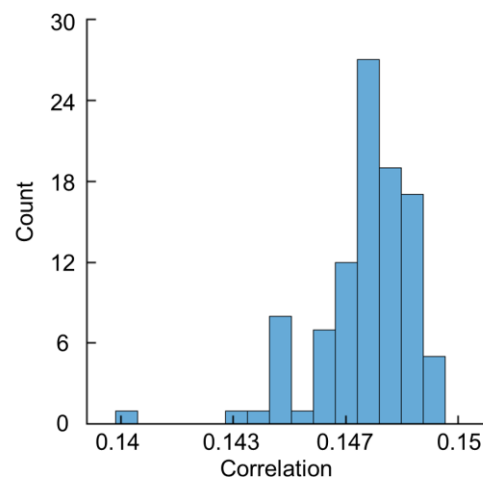

1199

1200 **Figure S2. Structural connectome is weakly correlated to the MEG-derived network of**

1201 **phase-synchronization** Histogram of correlations between MEG-derived network of phase-

1202 synchronization and 100 bootstrapped versions of structural connectome.

1203

1204

1205

1206

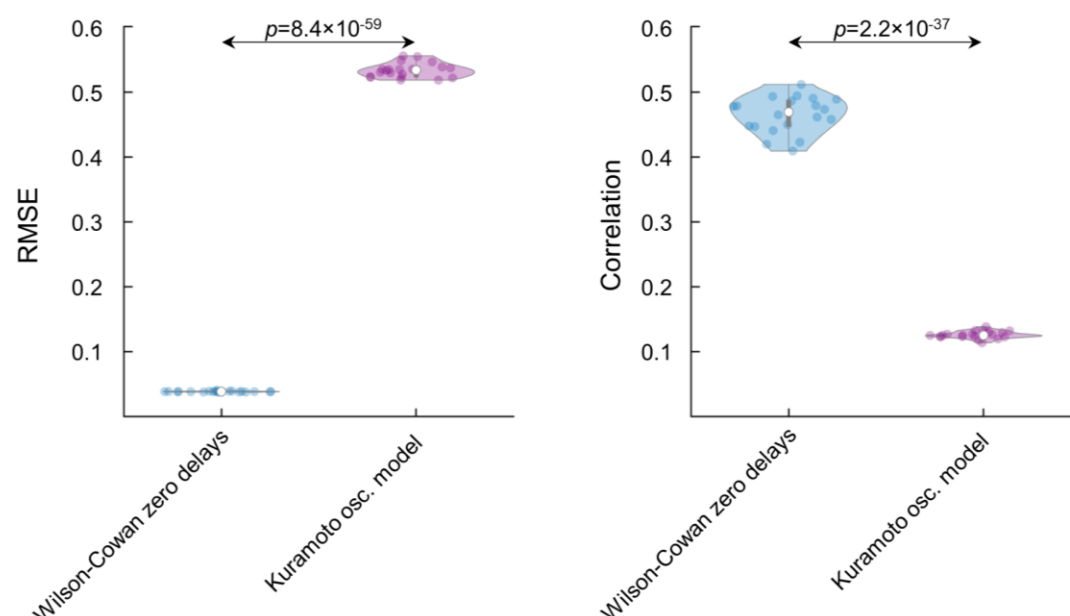1207

1208

1209

1210

1211

1212

1213

1214

1215

Figure S3. Wilson-Cowan zero delays model outperforms Kuramoto oscillator model a.
Violin plots of RMSE values for the Wilson-Cowan zero delays and Kuramoto oscillator
models (left panel). Violin plots of Correlation values for the Wilson-Cowan zero delays and
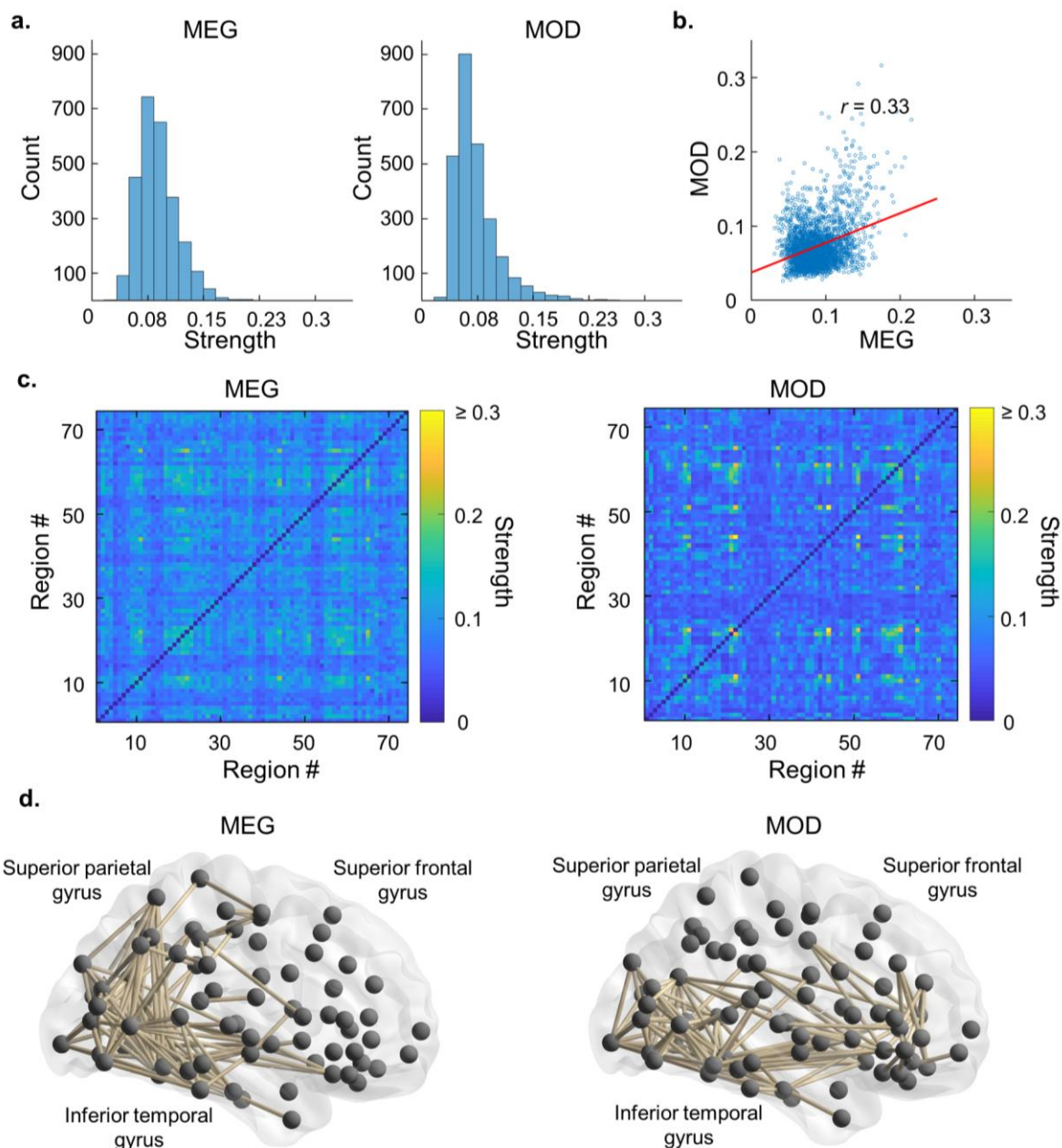Kuramoto oscillator models (right panel).

Figure S4. Moderate correspondence between mean model-generated network and right-hemispheric MEG-derived network of phase-synchronization a. Histogram of connection strengths for mean model-generated and right-hemispheric MEG-derived networks of phase-synchronization b. Scatter plot of connection strengths for right-hemispheric MEG-derived network of phase-synchronization against mean model-generated network of phase-synchronization c. Matrices of connection strengths between every pair of brain regions for mean model-generated and right-hemispheric MEG-derived network of phase-synchronization. d. Brain network visualisation of top 5 percentile strongest connections for mean model-generated and right-hemispheric MEG-derived networks of phase-

1244   synchronization. MOD = model. Brain networks were visualised with BrainNet Viewer

1245   (http://www.nitrc.org/projects/bnv/) (Xia et al. (2013)).